Biochimica et Biophysica Acta 1827 (2013) 1003–1019

Contents lists available at SciVerse ScienceDirect

Biochimica et Biophysica Acta

journal homepage: www.elsevier.com/locate/bbabio

Water oxidation mechanism in photosystem II, including oxidations, proton release pathways, O—O bond formation and O_2 release ☆

Per E.M. Siegbahn *

Department of Physics, ALBA NOVA, Stockholm University, SE-106 91, Stockholm, Sweden
Department of Biochemistry and Biophysics, Arrhenius Laboratory, Stockholm University, SE-106 91, Stockholm, Sweden

ARTICLE INFO

Article history:
Received 18 September 2012
Received in revised form 15 October 2012
Accepted 18 October 2012
Available online 24 October 2012

Keywords:
Density functional theory
Photosystem II
Oxygen evolving complex
O—O bond formation
Energy diagrams
Transition states

ABSTRACT

The present status of DFT studies on water oxidation in photosystem II is described. It is argued that a full understanding of all steps is close. In each S-transition, the manganese that is oxidized and the proton released are strongly implicated, and structures of all intermediates have been determined. For the S_2-state, recent important experimental findings support key elements of the structure and the mechanism. In this mechanism, the O—O bond is formed between an oxyl radical in the center of the cluster and an Mn-bridging μ-oxo ligand, which was suggested already in 2006. The DFT structure of the oxygen evolving complex, suggested in 2008, is very similar to the recent high-resolution X-ray structure. Some new aspects of the interaction between P_{680} and the OEC are suggested. This article is part of a Special Issue entitled: Metals in Bioenergetics and Biomimetics Systems.

1. Introduction

Water oxidation in Photosystem II has been one of the major questions remaining to understand in biochemistry. Until only a few years ago, a plausible mechanism for O—O bond formation was still missing, in spite of decades of advanced experimental studies, much depending on the lack of a geometric structure for the oxygen evolving complex (OEC). In 1999, modern quantum chemistry entered the field and the progress in the understanding has since then gradually increased both with the help of theory and experiments. The first major breakthrough occurred when the first X-ray structures appeared about a decade ago, although at quite low resolution of about 3 Å [1–3], and suffering from radiation reduction [4]. Still, these experiments have considerably helped to shed light on the structure of the oxygen evolving complex (OEC), which prior to that was limited to information obtained by EXAFS (Extended X-ray Absorption Fine-Structure) [5,6]. It can also be added that this EXAFS information was used in setting up the X-ray structures. In the initial stages of searching for a water oxidation mechanism, the leading suggestion for O—O bond formation was an attack by an outside water on an oxygen radical (or oxo group) bound to manganese [7–11]. In 2006, that mechanism was shown to be very unlikely, and a new mechanism was suggested where the O—O bond is formed in the center of the OEC from an oxygen radical and a bridging oxo-group [12]. The barrier was found to be at most half of the barrier of the old mechanism, 5–10 kcal/mol compared to 20 kcal/mol. Alternating spins for the four atoms directly involved was found to be a very important requirement. Still, the mechanism was obtained with a rather crude model of the OEC. Even though previous computational experience had shown that the general aspects of a mechanism are quite insensitive to details of the structure, the situation was not entirely satisfactory.

An important part of the further progress in finding a water oxidation mechanism was taken when it was realized that the significant problem of calculating *absolute* redox potentials and pK_a values using the present limited models could be circumvented in an accurate way [13–15]. It was realized that if the experimental driving force for water oxidation is used, only *relative* values were needed to construct most of the levels in the energy diagram. To construct also the other ones, one experimental value is required, see further below. There are obvious reasons to assume that the *relative* values should be accurately determined by a model of the present size (200 atoms), since the surrounding protein outside the model is expected to stay almost exactly the same, transition for transition. In contrast, there will be large contributions to the *absolute* values from charged residues even very far away from the OEC, but which will cancel for the relative values.

In 2008, the status of the structure of the OEC was considerably improved using DFT [13]. Using the information of the mechanism obtained [12] combined with the X-ray back-bone structure of the London structure [1] and the suggested ligand arrangements from the Berlin structure [2], a new structure was obtained, which has since

☆ This article is part of a Special Issue entitled: Metals in Bioenergetics and Biomimetics Systems.

* Tel.: +46 8 161263.
E-mail address: ps@physto.se.

0005-2728/$ – see front matter © 2012 Elsevier B.V. All rights reserved.
http://dx.doi.org/10.1016/j.bbabio.2012.10.006

then remained essentially the same in all the coming DFT studies. Last year a major experimental development took place when the first high-resolution structure at 1.9 Å was presented by Shen et al., which essentially confirmed the theoretical structure [16]. The main difference was that Asp170 was found to bind in a bridging mode between the terminal manganese and calcium instead of only terminally to the manganese as in the theoretical structure. The rest of the structure is very similar, including the critical positions of the outer manganese and the oxo groups, and the ligand connections. A minor problem with the X-ray structure is that it is probably reduced by X-rays, indicating that it is unlikely to be in the S_1-state as originally claimed.

A comparison of the core parts of the different structures are shown in Fig. 1. The orientation of the structures were made such that one Mn-atom of the structures compared is placed at the same position and two other as close as possible to each other. This avoids bringing in an irrelevant rotation between the complexes. The most striking differences between the DFT structure [14] and the London structure, is the positioning of the outer manganese, which differs by 3.2 Å. In the DFT structure, the outer manganese is connected to the cube by two μ-oxo bridges, while in the London structure it is only connected to one of the bridging oxos in the cube. There is also an additional oxo bridge between the Mn-atoms in the theoretical structure. A similar, significant but smaller, difference is seen in the comparison to the Berlin structure, where the positioning of the outer manganese differs by 1.4 Å. The positions of the oxo-bridges were not suggested in the Berlin structure due to the low resolution, but a single oxo-bridge to the outer manganese can be assumed based on the Mn–Mn distance of 3.3 Å. In the DFT structure, the long Mn–Mn distance of 3.3 Å is instead within the cube. On the other hand, the positioning of the outer manganese and the oxo-bridges between the manganese atoms in the recent high-resolution Shen structure are very similar to the DFT structure. In the comparison, it should be

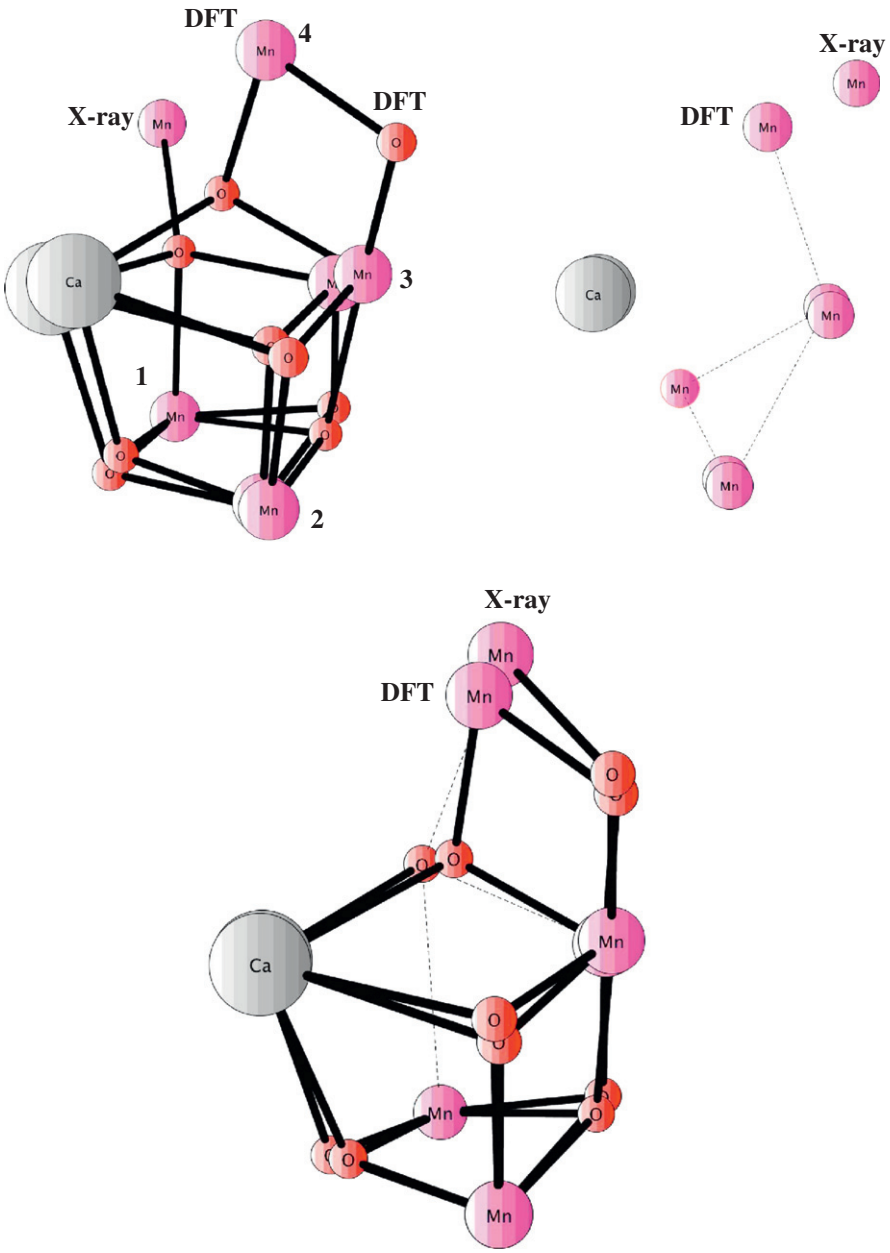

Fig. 1. Comparison of the DFT structure with the London structure (upper left), the Berlin structure (upper right) and the Shen structure (bottom). For the comparison to the Berlin structure no oxygens are given since they were not suggested in that structure. To clarify which atoms belong to which structure, the atoms are labeled **DFT** and **X-ray** when the positions are significantly different.

remembered that the Shen structure is most probably reduced by X-ray radiation. As will be seen below, the region between the outer manganese and the cube is the region where most likely O—O bond formation takes place according to the present DFT studies. In particular a sufficiently open space in this region is necessary for a low-barrier mechanism. This is precisely the region where the low resolution structures are incorrect and these structures have therefore mainly led to suggested water oxidation mechanisms that according to DFT comparisons are significantly wrong [12], which has actually been the case also for suggestions based directly on the high-resolution structure [16]. The mechanism that has been suggested based on the X-ray structures is an attack on an oxo-group by an external water or a water bound to calcium. Other mechanisms involving an oxyl radical could also be mentioned here. The first suggestion of a radical mechanism was made by Yachandra et al. [5], in which a bridging oxyl radical was proposed to be formed already in S_3. The O—O bond should then be formed between this oxyl radical and the other oxo-group, bridging the same centers. A mechanism suggested by Messinger [17] starts out similarly with a formation of a bridging oxyl radical in S_3, but the O—O bond is not suggested to be formed involving this oxygen. Instead, one of the oxygen involved in forming the O—O bond is another bridging oxo ligand, while the other oxygen is bound terminally to **Mn4**. Notably, the involvement of a bridging oxo-ligand is similar to the mechanism suggested by DFT.

The past three years, progress has continued. First, the old DFT structure was updated with the new information from the high-resolution X-ray structure, which essentially meant moving Asp170 slightly [18]. A transition state was optimized for the new structure, almost identical to the old one, with alternating spins, similar key distances and barrier height. As expected, the different positioning of Asp170 has nearly no effect. Later on, pathways in the OEC were obtained for moving the protons from the substrate to the start of the protein transfer chain at Asp61 [19]. Some of the most important recent results have been obtained by a combination of spectroscopy and theory. Based on the new X-ray structure and old DFT structure, using EPR, ENDOR, and DFT, a detailed structure of the OEC in the S_2 state was reached [20] that agrees almost perfectly with a structure obtained independently by energy minimization [18]. The positions of the oxo groups and the protonation states, even including which ligands are water and which are hydroxides, agree, also which manganese is Mn(III) at that stage. The structure is very similar to the one suggested for the S_2-state in 2008. Quite recently, also the substrate oxygen positions have been determined for S_2 using a W-band ^{17}O-ELDOR detected NMR spectroscopy [21]. These positions agree with the ones suggested by the DFT study [12–14,18,19], but disagree with all other previous proposals except the one by Messinger [17]. Overall, even after these experiments, there is not a single example yet of where the present energy minimization did give a result that is inconsistent with any spectroscopical results. However, since the DFT method and the model are not exact, minor deviations must be expected in the future. Large, significant energy deviations become less and less probable as more tests are made.

In the present paper, the previous studies are continued by presenting the complete set of proton and electron release steps. Water binding, O—O bond formation and O_2 release are also described. The calculations follow a recent study where the S_2 to S_4 transitions were studied in detail [19]. This means the determination of a large number of transition states, most of them describing the steps of proton transfer until the proton reaches Asp61, from where it is released to the bulk [3,22,23]. At the present stage, no major changes of the mechanism for water oxidation are expected in the future.

For completeness, other theoretical work, some of which has led to other suggestions, should be mentioned. Other experimental work will be discussed in the text below. For theoretical work done until recently, there has been a review where other references can be found [24]. Cluster models and mechanisms have been studied by Pace et al. [24]. They suggest lower oxidation states than the ones suggested here and in most other studies. They base their conclusions on a computational analysis of NEXAFS (Near Edge X-ray Absorption Fine-Structure) spectra using a TDDFT (Time Dependent DFT) approach. In a recent study it has been questioned if the TDDFT method is accurate enough for the analysis, and also if NEXAFS (or XANES) is really a reliable technique for determining oxidation states [25]. Given the close contact between the Mn-atoms in the OEC, it would be extremely surprising if the low oxidation suggestion, could produce a reactive state in S_4, since an oxygen radical has to be close to an Mn(III) center. It is also difficult to understand why the oxidation process should be interrupted before all possible Mn(III) to Mn(IV) oxidations have been performed. This would be contrary to all experience from biomimetic systems. In 2007, Kusunoki [26] suggested a structure for the S_0-state based on the Berlin structure [2], with the same correct and incorrect aspects as that structure. The ligands are at essentially the correct place, but the outer manganese is too far out, connected to the cube by only one oxo-ligand and having three water ligands, two of which were suggested to be the substrates based on water exchange considerations. In 2011, after the high-resolution structure, the model was refined. The originally suggested mechanism was kept, now supported by EXAFS calculations. To explain the unusual position of the central oxo-ligand, it was suggested that there are two different structures for the S_1-state with equal energy [27]. In contrast to the cluster approach, the QM/MM (quantum mechanics/molecular mechanics) method has been used by Batista et al. [28,29]. They restricted the structures investigated to be similar to the one of Ferreira et al. [1]. For the best structure obtained they also did an analysis of EXAFS spectra [30], and found that their suggested structure would match the experimental spectrum if it was only slightly modified. They took this information to be a confirmation of their suggested structure. After the new X-ray structure by Shen et al. appeared, it became clear that their suggested structure was quite different from the real structure. Later on it has been shown that, using their type of analysis, also other quite different structures match the EXAFS spectra well [31]. Furthermore, Batista et al. suggested an O—O bond formation mechanism that is different to the one proposed here. A nucleophilic attack from an external water (or bound to calcium) was suggested to form the bond with an oxygen radical bound to manganese. Their mechanism is the same as the one suggested earlier in several DFT studies starting 1999 [11–15], but which was demonstrated to lead to too high barriers in a study 2006 [12]. Even earlier than that, this mechanism was suggested in several experimental papers [32,33]. Neese et al. [34] used a spectroscopic DFT approach to investigate several types of clusters. They suggested that three of these structures, including the previous theoretical structure [13], which were found to match EPR spectra best, would be most similar to the real structure. In a later study [35], but before the high-resolution structure appeared, it was shown using an energy minimization approach that the structure suggested by Batista et al., and all the new structures studied by Neese et al., were energetically quite far above the DFT structure mentioned above, and therefore had to be mechanistically different from the real structure. Actually, the same conclusion could be made for all four structures suggested by polarized EXAFS [36], which were concluded to be significantly too high energetically [14]. However, as a general type of structure, the EXAFS-III model has similarities to the DFT suggested structure, with three short Mn–Mn distances, two of them in the cube. It can be described as a mirror-image of the DFT structure. The mirror image leads to another assignment of the oxidation states and forces two of the manganese centers to be 5-coordinated, if water ligands are not added to fill the empty positions. The general structure suggested by Dau et al., also based on EXAFS (including a molecular mechanics modeling), is more similar to the DFT structure [37]. However, only one short Mn–Mn distance was suggested in the cube. At that point Cox et al. [38] did a new more extended DFT analysis and concluded that the previous DFT structure [13] matched the experimental multifrequency EPR and ^{55}Mn-ENDOR spectra best. Simultaneously,

and independently, Kaupp et al. [39] reached the same conclusion. With the appearance of the high resolution structure this conclusion was definitely confirmed. Quite recently, Batista et al. have analyzed the protonation state of the S_1-state of the Shen structure [40]. They concluded that the Shen X-ray structure is a mixture of oxidation states. A similar conclusion was reached also in other recent studies [18,20,41,42]. In another study [43], Batista et al. analyzed the role of chloride by deleting it, and concluded that one role might be to prevent salt-bridges which would hinder proton transfer. Other more direct effects on the redox potentials and pK_a values were not considered.

2. Methods and models

The Density Functional Theory (DFT) calculations discussed here were performed in the same way as described in detail previously [19]. The hybrid functional B3LYP* [44,45] was used with polarized basis sets for the geometries (lacvp*), large basis sets for energies (cc-pvtz(-f)), and a surrounding dielectric medium with dielectric constant equal to 6.0 (basis lacvp*). The performance of the B3LYP functional for the present type of problems has been reviewed [46–48], indicating a typical accuracy within 3–5 kcal/mol, normally overestimating barriers. Dispersion effects were added using the empirical formula of Grimme [49]. A difference to the previous study is that zero-point effects were calculated using large, but truncated, models of the present structures, including about 100 atoms. The truncations were made by deleting atoms on the amino acids outside the main group (His modeled by imidazole, Glu, Asp by formates) and freezing the end-point hydrogen atoms. The lacvp basis set was used. Fully optimized transition states were located at the same computational level, and the important (varying between one and three) distances were transferred to the large model where they were fixed, during another full geometry optimization. The calculations were performed with the Jaguar program [50].

The quantum chemical cluster model chosen for the present applications is the same as the one used in the most recent study [19]. The model is based on the high-resolution (1.9 Å) structure by Shen et al. [16], and is seen for the S_2-state in Fig. 2, where only the most important atoms are shown. The full 200 atom structure is given as Supplementary material. The amino acids included in the model are first the directly binding amino acids, Asp170, Glu189, His332, Glu333, Asp342, Alal344 and Glu354. The second shell residues Asp61, His337 and Arg357 and the region around the chloride are also included. This region contains, besides chloride, also Lys317 and three water molecules, forming a hydrogen bonding network, as in the X-ray structure.

The energy diagrams discussed below are constructed following a scheme described previously, where only relative pK_a and redox potentials are used, see for example Ref. [51]. First, the absolute energy to remove an (H^+,e^-)-couple from the OEC and place them at the respective acceptors, water and P_{680}, was chosen to fit what is known experimentally about the driving force for the entire reaction. This fixes every second energy level in the diagram from the calculated relative energy (H^+,e^-) differences. To fix also the other half of the energy levels, one additional parameter has to be chosen. How this parameter was chosen here is described below. Finally, a spin-correction of −2.8 kcal/mol was added for the S_4-state structures. This correction was obtained from using a Heisenberg spin-Hamiltonian formalism [52] for the S_4^{-1} oxygen radical state.

3. Results

In a recent study, two of the S-transitions, S_2 to S_3 and S_3 to S_4 were studied and described in detail [19]. An important difference compared to the previous study is that it was here found necessary to add a proton to His337. This does not markedly change the relative energies, which are the only ones used in the diagrams, except for the step when O_2 is released, see further below. Since the mechanism remains exactly the same with the added proton for the two transitions already discussed, only the new energies for these transitions are given below. The relative energies are very similar to the previous ones given. For all transitions, to move the protons from the center of the cluster, where the chemistry should occur in the present mechanism, requires a hydrogen bonding network connecting the center with Asp61, from where the proton moves to the bulk [3,22,23]. Most of the required network between

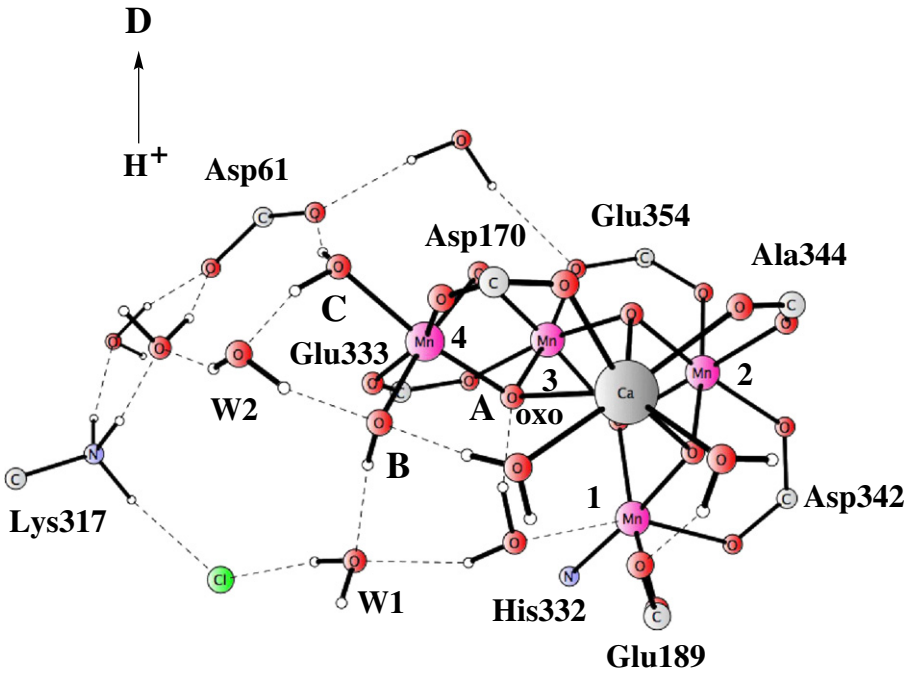

Fig. 2. Optimized S_2^0-state. **1–4** are the numbering of the Mn-centers, while **A–D** label the different positions of the proton during release. **W1** and **W2** are second shell water molecules used during proton transfer. Only most essential atoms are shown.

the center and Asp61 is present in the high-resolution structure [16], see Fig. 3, but reoptimizations are required for each step of the process.

The proton transfer pathway from the center of the OEC complex to Asp61 is shown in Fig. 2 for the S_2-state. The metal atoms are labeled **1–4** as in the high-resolution X-ray structure. Four positions along the proton transfer pathway are labeled **A–D**. The water in position **A** on **Mn1** is the starting point for the transfer. From **A**, a proton should first move to the hydroxide in position **B** on **Mn4**. The next step is a proton transfer between positions **B** and **C** on the same **Mn4**. From position **C** a proton can then reach Asp61 which is the starting point for the proton transfer path from the OEC to the lumen. **D** represents a point in the lumen, where the proton is dissolved in water at pH 7. (It should be observed that in a release of a proton, it does not need to be the same proton that is involved in each step of this process). The proton cannot move directly between the different positions **A–C** but needs help by the waters labeled **W1** between **A** and **B**, and **W2** between **B** and **C**. Lys317 and Asp61 are critical residues along the pathway, where also the chloride has a role. In some transitions also a third water (**W3**) is needed. Chloride has still another H-bond to the N-H backbone of Glu333 (this bond is not shown in the figures). The rest of the amino acids are essentially only spectators on the side of the transfer pathway, but play roles as charged groups, like the metal atoms and oxo groups. In each optimized structure the total gas phase binding energies of the water molecules have been calculated and compared to the empirical value of 14 kcal/mol, which is the binding of a water molecule in bulk water. In principle, when the calculated gas phase binding energy (X kcal/mol) is smaller than 14 kcal/mol, (14-X) kcal/mol should be subtracted from the energies, but this did not occur for any water in the present structures.

3.1. The experimental driving force

To obtain the experimental driving force for the entire process of water oxidation, the redox potentials for P_{680} and oxygen are needed. At pH = 7 the redox potential for forming O_2 from water is 0.8 V. For P_{680} a redox potential for the resting state has been measured to be 1.25 V [53,54], the largest one in biology. In previous studies, the redox potential of P_{680} has been assumed to be the same for all S-states leading to a total driving force for water oxidation of 41.5 kcal/mol [14]. However, a combination of certain experimental observations now lead to the conclusion that this assumption is not entirely correct. The first observation is that only an electron leaves the OEC in the S_1 to S_2 transition [60,61]. This means that the charge of the OEC in the S_3 and S_4 states becomes one plus-unit larger than the one in S_0, S_1 and S_2. The key question here is if the increased charge of the OEC has any measurable effect on the redox potential of P_{680}. Since the distance between the Mg-centers of P_{680} and the OEC (taken to be the outer Mn) is as large as 18 Å, the answer to this question is not obvious. However, an observation in the S_3 to S_4 transition suggests that the effect should be substantial [55,56]. It has been found that when P_{680} is oxidized, an electron is transferred from Tyr_Z and after that a proton is expelled from the OEC. Since no mixing between protonated and unprotonated states are observed in the experiment, before or after P_{680} oxidation, this means that the proton on the OEC should be bound by at least 2.5 kcal/mol before P_{680} oxidation, and afterwards the same proton should leave the OEC exergonically, again by at least 2.5 kcal/mol. Altogether, this leads to an effect from P_{680} oxidation of at least 5.0 kcal/mol on the pK_a of the proton on the OEC. The reverse effect must obviously be the same, i.e. the effect on the redox potential of P_{680} by the additional proton on the OEC must be at least 5.0 kcal/mol (0.22 V). This means that the redox potential of P_{680} in the S_3 and S_4 transitions should be as high as 1.47 V (1.25 + 0.22), which significantly helps the final critical steps of water oxidation. Thermodynamically, the creation of the high redox potential is not a problem since the energy of the photon is 1.84 V. The price paid is instead that the back-reaction, leading to a loss of the charge separation, becomes much easier in S_3 and S_4. Indeed, it has been observed that the miss parameter of flash-induced O_2 evolution is higher in the S_2 to S_3 and S_3 to S_0 transitions as compared to the earlier S-transitions [57,58]. An interesting aspect of the increased redox potential of P_{680} in the late S-transitions is that the additional driving force is not used to make OEC oxidation easier, as one might intuitively think, but rather to make proton release easier. In summary, the total driving force for water oxidation becomes 51.5 kcal/mol (41.5 + 2 × 5.0), and this is the value used in the diagrams discussed below.

From the effect of 5.0 kcal/mol of P_{680} oxidation on the pK_a of the proton on the OEC, an average dielectric constant of the protein can be estimated. If the distance of 18 Å mentioned above is used, the dielectric constant becomes 3.1. However, if an edge to edge distance of 12 Å is used instead, the dielectric constant becomes 4.6. Both these estimates may be considered to be surprisingly low, but such a low dielectric constant is needed to reproduce the experimental observation. Interestingly, a quite similar dielectric constant of only 3–4 has been shown to be needed to reproduce measured pK_a differences in cytochrome c oxidase [59].

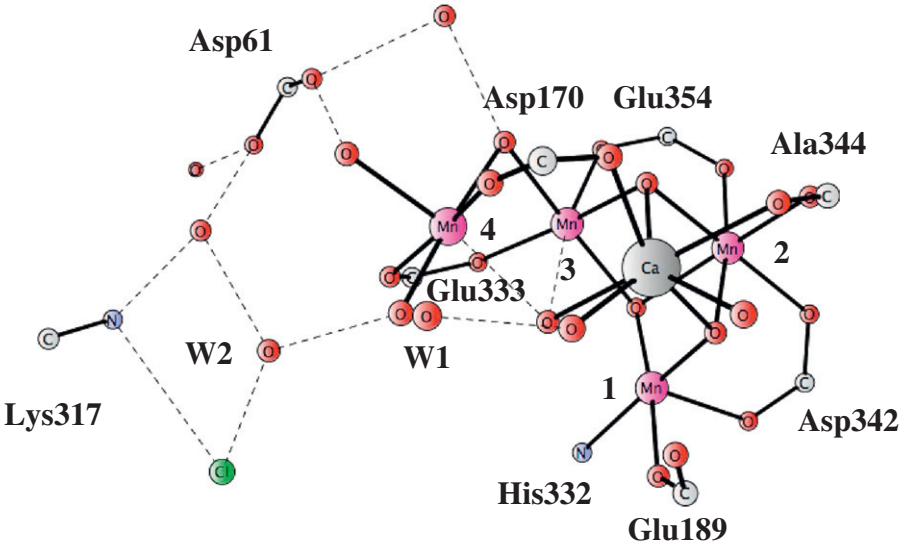

Fig. 3. Proton transfer region of the high-resolution X-ray structure [16]. **1–4** are the numbering of the Mn-centers. **W1** and **W2** are second shell water molecules used during proton transfer. Only most essential atoms are shown.

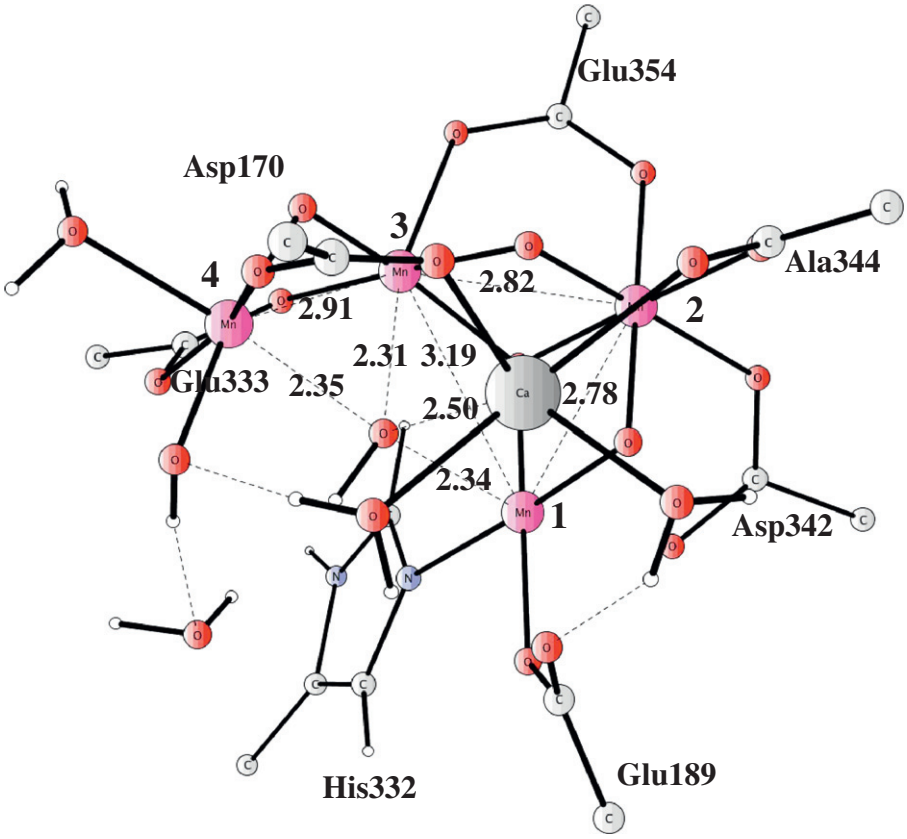

Fig. 4. The optimized S_0^{-1} state. The Mn–Mn and the Mn–OH distances between the central OH group (**O5** in the X-ray structure) to the manganese and calcium atoms are given in Å. Only most essential atoms are shown.

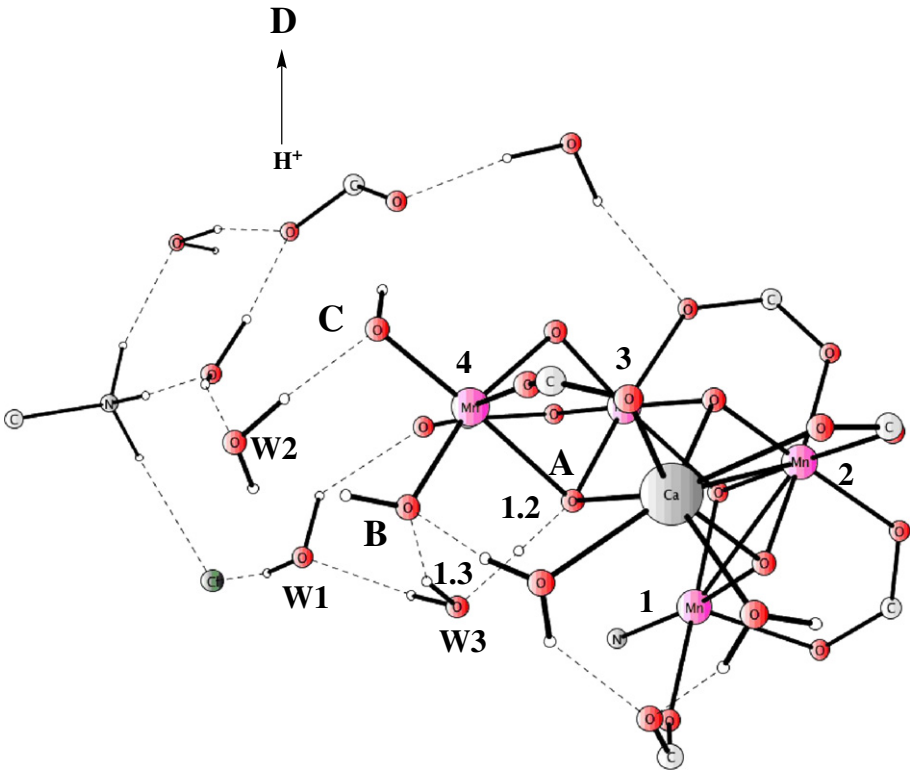

Fig. 5. Optimized TS-structure for the first proton transfer in the S_1^{-1} state. Only most essential atoms are shown.

The oxidation of Tyr_Z by P_{680} does not give any additional driving force for the expulsion of the proton on the OEC. The increased repulsion on the proton on the OEC obtained by moving the electron from Tyr_Z to P_{680}^{+} is exactly counterbalanced by the increased cost for moving the electron due to the proton on the OEC. Instead, moving the charge from P_{680}^{+} to Tyr_Z could give a kinetic effect that could help the expulsion of the proton.

To construct full energy diagrams, as described in detail in other papers [13–15], one experimental energy value is needed. As in the recent paper [19], this value is taken from the detailed experimental knowledge of the initial part of the S_3 to S_4 transition as described above. Removing the proton for the S_3-state is fitted to be endergonic by 2.1 kcal/mol.

3.2. The S_0 to S_1 and S_1 to S_2 transitions

The S_0 to S_1 transition starts out at the optimized S_0-structure shown in Fig. 4. This structure has an unusual feature and this is the position of the hydroxide in the center of the complex. The Mn–OH distances are quite long with 2.34, 2.31 and 2.35 Å. Interestingly, the X-ray structure has a similar position for the **O5**-oxygen. One condition for having such a structure is that all manganese centers involved should have oxidation states not higher than Mn(III). If anyone of the manganese atoms are oxidized to Mn(IV), the hydroxide would directly move towards that manganese and form the usual bond of around 1.9 Å. The only Mn(IV) at this stage is thus **Mn2**. From this it is clear that the X-ray structure observed cannot be in the S_1-state as claimed, since this would require that one of the manganese binding to the hydroxide would be an Mn(IV). The X-ray structure therefore has to be reduced at least to the S_0-state by X-ray radiation. Another condition for the unusual Mn–OH distances is probably the rather close interaction with calcium with a distance of 2.50 Å, see figure. The Mn–Mn distances in the optimized S_0-structure are **Mn1**–**Mn2** = 2.78 Å (2.8 Å), **Mn1**–**Mn3** = 3.19 Å (3.3 Å), **Mn2**–**Mn3** = 2.82 Å (2.9 Å), and **Mn3**–**Mn4** = 2.91 Å (3.0 Å), where the X-ray distances [16] are given in parenthesis. From the

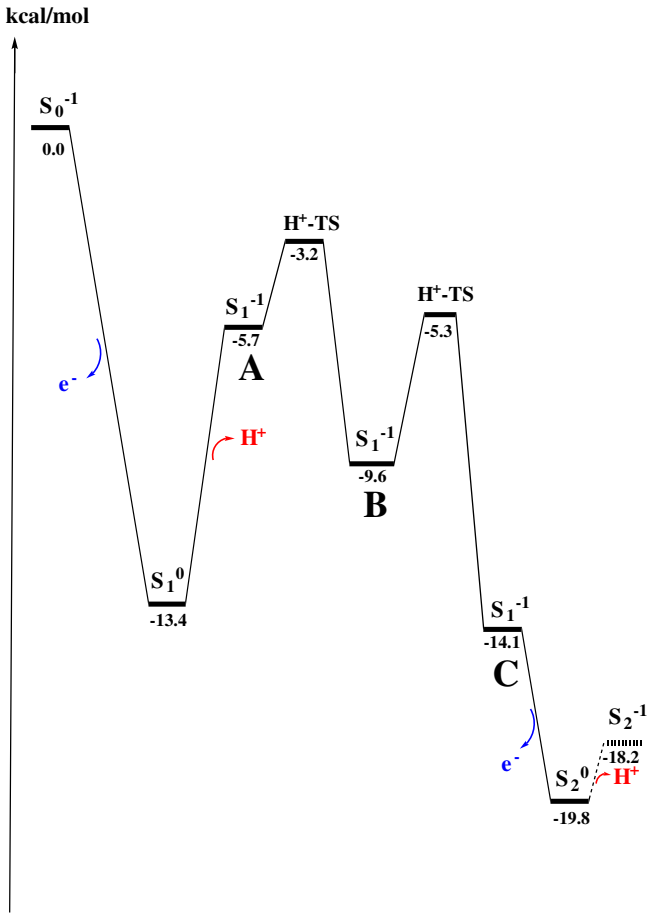

Fig. 7. Energy diagram for the S_0 to S_1 and S_1 to S_2 transitions. The labels **A–C** indicate the positions of the moving proton, see Fig. 2.

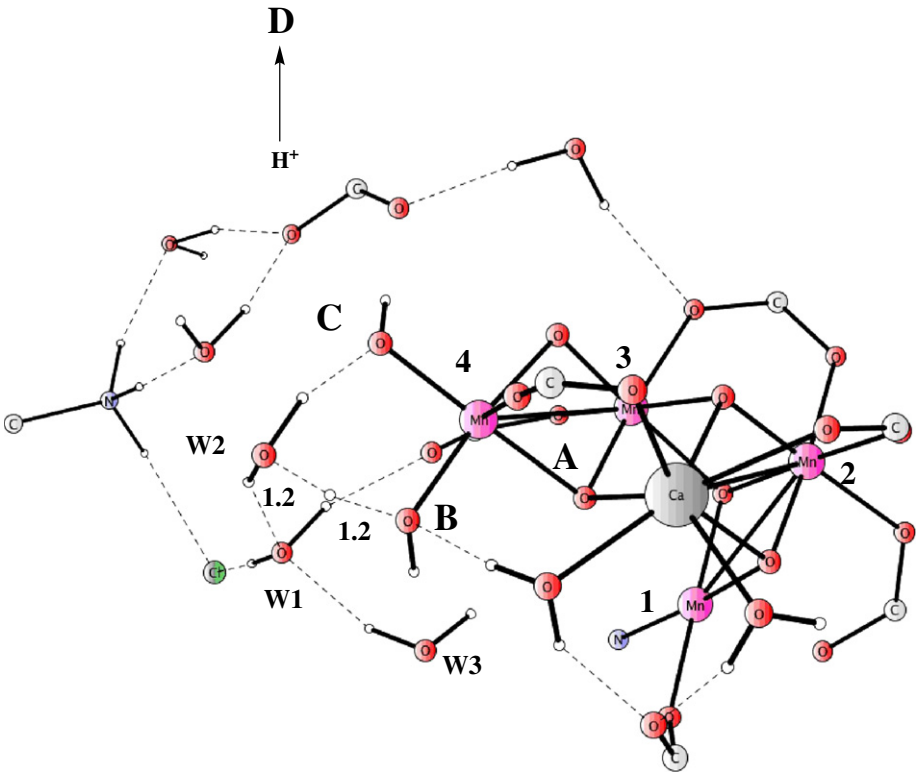

Fig. 6. Optimized TS-structure for the second proton transfer in the S_1^{-1} state. Only most essential atoms are shown.

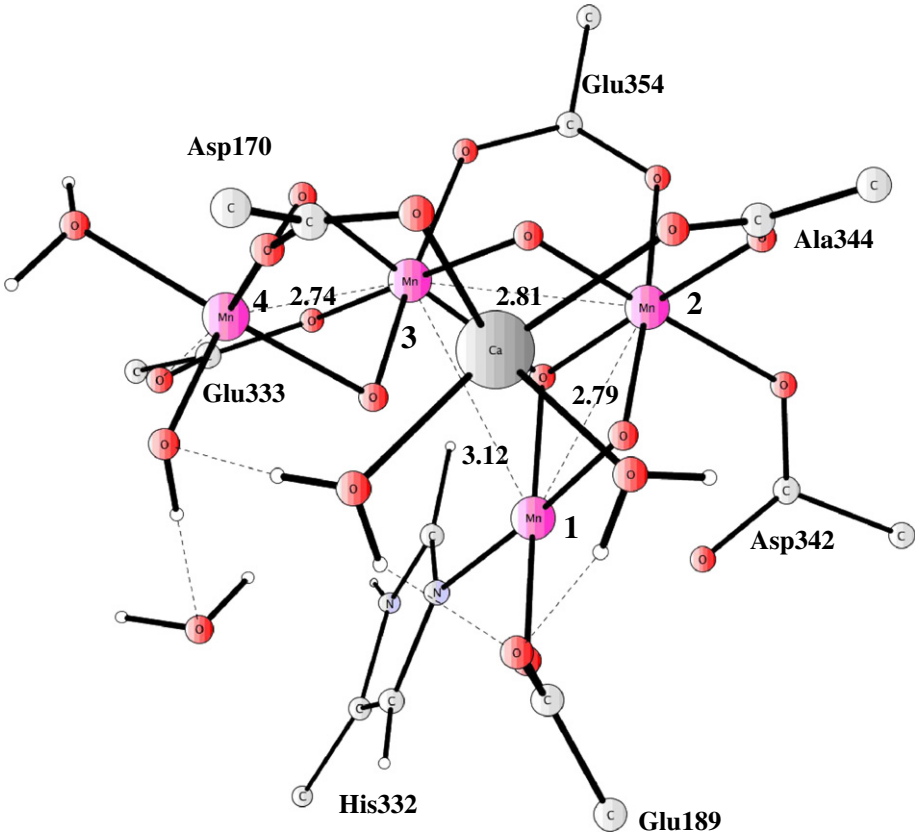

Fig. 8. The optimized S_1^{-1} state. Only most essential atoms are shown.

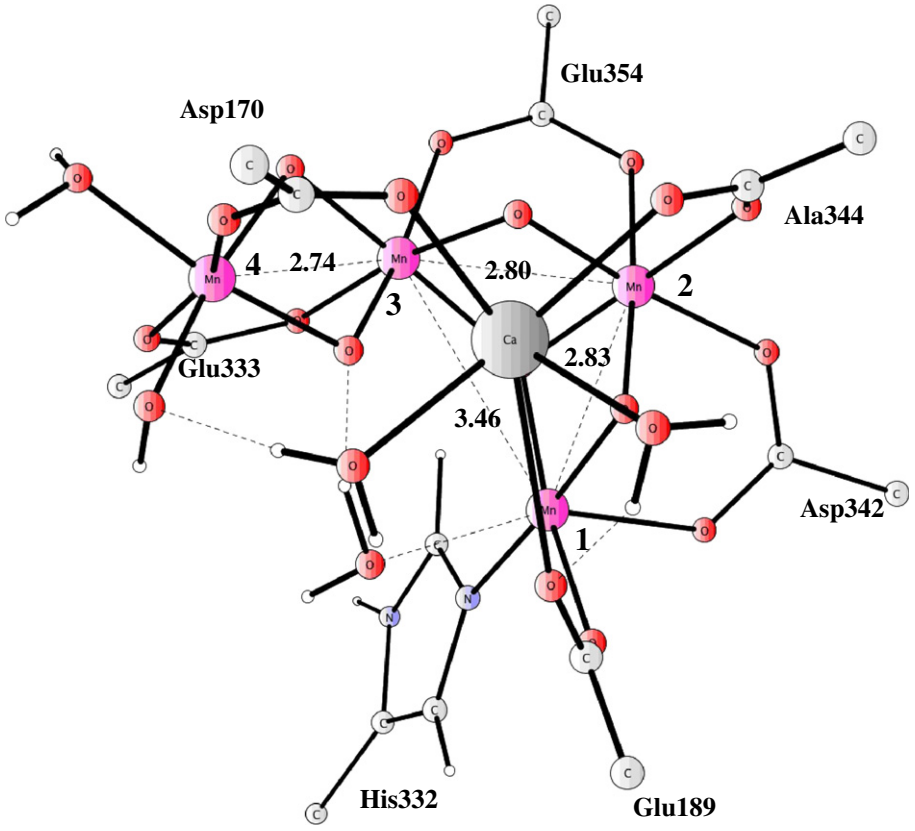

Fig. 9. Optimized S_2^0 structure. Only most essential atoms are shown.

large similarity between the present S_0-structure and the X-ray structure, it is tempting to conclude that the latter should be in an S_0-state. However, other suggestions are also possible, like a mixing of different reduced states [41,42]. A very different suggestion is that the X-ray structure should be a mixing of two S_1-structures with exactly the same energy [27]. Since this would rely on a remarkable coincidence and that X-ray reduction should not be present, the latter suggestion appears less likely.

The transition to the next S-state occurs in many steps, as also described recently for the higher S-transitions [19]. The first step is a strongly exergonic electron transfer from the OEC to P_{680}^+ of 13.4 kcal/mol. As usual, the electron release starts by transferring an electron from Tyr_Z to P_{680}^+, which is followed by an electron transfer from the OEC to Tyr_Z^+. The oxidized center is **Mn3**. After the electron release there is an endergonic proton release of 7.7 kcal/mol. The proton is released from the water on the outer manganese, **Mn4**. The position of one of the protons in this initial S_1^{-1}-state is not optimal, which leads to two additional proton transfers. The TS for the first one is shown in Fig. 5. This step moves a proton from the central hydroxide at **A** to the hydroxide on **Mn4** (position **B**), with a barrier of only 2.5 kcal/mol and an exergonicity of 3.9 kcal/mol. As seen in the figure, water **W3** is involved in the transition. The TS for the second proton transfer step is shown in Fig. 6. In this case a proton is moved from the water ligand just formed on **Mn4** at position **B** to the hydroxide on the same manganese at position **C**, formed directly after proton release. The barrier for this step is also low with only 4.3 kcal/mol, and the step is exergonic by 4.5 kcal/mol. Water **W3** is involved in the transition. These proton transfers lead to the suggested S_1-state, shown in Fig. 8. The energetics of the S_0 to S_1 transition is shown in Fig. 7. With the present parametrization it can be noticed that the S_1^0 and the final S_1^{-1} states are very close in energy with −13.4 and −14.1 kcal/mol, respectively. From the calculations alone this energy difference is too small to conclusively determine which state is the ground state for S_1. However, experimentally it is quite clear that only an electron leaves the OEC in the S_1 to S_2 transition [60,61], which means that the S_1 ground state has to be an S_1^{-1} state. From the calculations it should be the one with the proton in position **C**.

The optimized S_1 ground state is shown in Fig. 8. The Mn–Mn distances are **Mn1**–**Mn2** = 2.79 Å (2.8 Å), **Mn1**–**Mn3** = 3.12 Å (3.3 Å), **Mn2**–**Mn3** = 2.81 Å (2.9 Å), and **Mn3**–**Mn4** = 2.74 Å (3.0 Å), with the X-ray distances [16] in parenthesis. As already discussed above, these distances do not match the experimental ones very well. In particular, the experimental **Mn3**–**Mn4** distance is too long by 0.2–0.3 Å, indicating that one of the experimental bridging oxo-groups is protonated. This is also the distance that changes most between the S_0 and S_1 states, for the same reason. There is also a notable change of the long **Mn1**–**Mn3** distance, but this distance is more sensitive to details and the change is not as significant. The description of the OEC with three short and one longer bond, as indicated in one EXAFS study [62–64] is more clear in the S_1 than in the S_0 state. The EXAFS distances obtained were three with 2.7 Å distances and one with 3.3 Å. The accuracy of the present methodology is not higher than this discrepancy between theory and experiments. In another EXAFS study [6], only two short Mn–Mn distances were suggested.

To reach the S_2-state, **Mn4** is oxidized to Mn(IV). The transition is exergonic by 5.7 kcal/mol. The structure, see Fig. 9, is very similar to the one of the S_1-state. The Mn–Mn distances are **Mn1**–**Mn2** = 2.83 Å (2.79 Å), **Mn1**–**Mn3** = 3.46 Å (3.12 Å), **Mn2**–**Mn3** = 2.80 Å (2.81 Å), and **Mn3**–**Mn4** = 2.74 Å (2.74 Å), with the calculated S_1 distances in parenthesis. Of the short distances only **Mn1**–**Mn2** changes with a lengthening of 0.04 Å. From EXAFS, no significant distance changes were observed, but it is not clear if such a small lengthening would be observable with three Mn–Mn distances of similar size. The longer, much more sensitive, **Mn1**–**Mn3** distance increases by as much as 0.3 Å, which has not been indicated by EXAFS, but to obtain this distance accurately is more difficult both experimentally and theoretically. The second substrate water can also be seen in the figure. It is now very weakly bound to **Mn1** with an Mn–O distance of 2.4 Å. This result is in agreement with water exchange experiments by Hillier et al. [65], that indicate at most a very weakly bound substrate water in S_2. It is also in agreement with suggestions by Dau et al. [6], who suggested that **Mn1** is 5-coordinated at this stage with the sixth ligand not closer than 2.4 Å. More recently, strong support for 5-coordination has been demonstrated by Mn ENDOR data [38].

An important part of the S_1 to S_2 transition is indicated at the end of the curve in Fig. 7. This part shows that a release of a proton at that stage is endergonic by 1.6 kcal/mol, which means that the proton will stay at the OEC when P_{680} is oxidized the next time, which significantly increases the driving force for the next step, as discussed above. It should be noted that the parametrization (a single parameter) of the energetics was not taken from this transition but for the next one with S_3 to S_4. The substrate water is not bound in S_1, but a tentative place for it outside the OEC is still shown in Fig. 8.

There have been several interesting experimental and theoretical studies on the S_2-state recently. It has been known for decades, that two different spin-states of S_2 can be observed. One of them has an EPR, g = 2.0, multiline signal [66], while the other one has a high spin, g ≥ 4.1, signal [67]. In one of the recent studies, two interconvertible structures of S_2 were demonstrated, and identified as corresponding to these spin-states [68]. The energy difference of these states was found to be only 1–2 kcal/mol, depending on the functional. The result using the present model is quite similar with 3.4 kcal/mol. In previous optimizations of the S_2 structure, the results converged to any one of these structures depending on the starting coordinates, but always with the same order of the states [14].

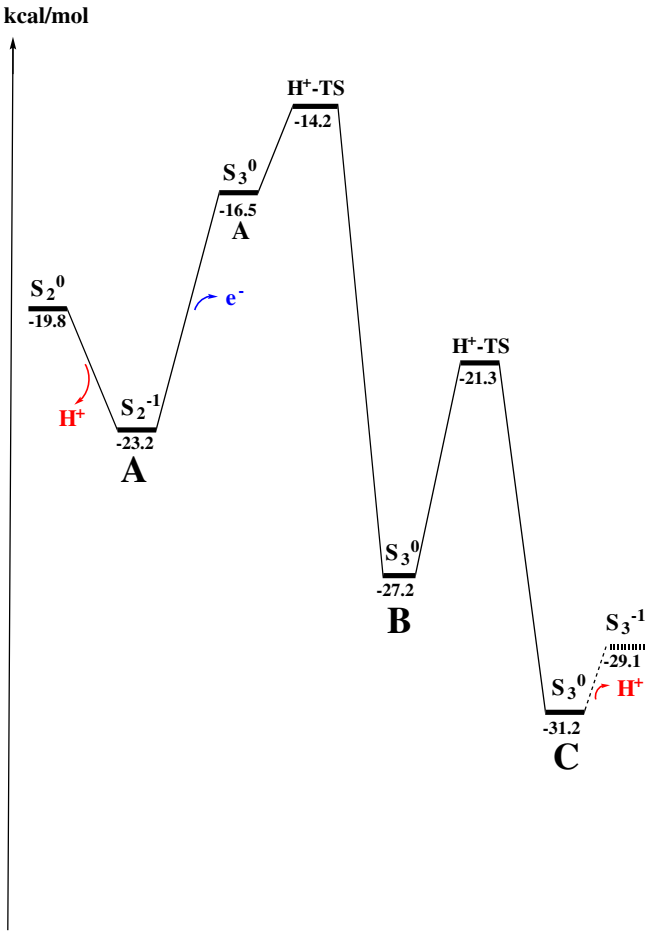

Fig. 10. Energy diagram for the S_2 to S_3 transition. The labels A–C indicate the positions of the moving proton, see Fig. 2.

In a combined theoretical and experimental study a structure for the S_2-state was reached [20], which is essentially identical to the one reached using the present model [18]. This DFT structure was found to match the experimental multifrequency EPR and ^{55}Mn–ENDOR spectra well. A major experimental breakthrough was reached in another study by the same group [21]. They were able to show which oxygen in the S_2-state that are most likely to form dioxygen, by a combination of ELDOR and water exchange experiments. The interpretations were built on earlier water exchange experiments [32,65,69,57], where one substrate water was found to exchange very slowly and one very fast in S_2. The slowly exchanging oxygen was in the new study proposed to be one of the central oxo-groups in agreement with the DFT mechanism [13,14,18]. The second substrate water was suggested to bind in connection with formation of the S_3-state, as also suggested by the present DFT model. These results are at variance with the conclusions of an earlier experimental study on model systems and manganese catalase, where water exchange for an oxo group was found to be very much slower than the slow water exchange in OEC, suggesting that an oxo group could not be a substrate [70]. At present, water exchange pathways in S_1 and S_2 have almost been determined using the present DFT model. For the pathways found so far, the direct water exchange only occurs for a water on a Mn(III) center. This means that the rate of exchange for another type of water derived ligand depends on the ease of transferring electrons and protons and sometimes moving the water to create that situation. This means going over sometimes several transition states before the direct water exchange. The calculations indicate that it is somewhat easier in S_2 than in S_1. Qualitatively, the results are in line with the ELDOR experiments [21]. Some further work is required and will be presented elsewhere.

3.3. The S_2 to S_3 transition

The proton transfer steps in the S_2 to S_3 transition were already discussed in detail in the previous paper [19]. Only the differences compared to the previous study, which mainly concerns the energetics, will therefore be discussed here. These differences are related to the protonation of His337, and, more importantly, to the new analysis of the P_{680} reduction as described above. The new energetics is shown in Fig. 10.

The mechanisms for the internal proton transfers on the OEC are structurally essentially identical to the ones in the earlier study, involving the same ligands and the same intermediate waters. The energetics of these steps are also very similar. Two new transition states were obtained, this time based on fully optimized structures for a smaller model including only the main groups of the side chains. The main distances from the small model were then held fixed for the large model. The previous procedure, where the key distances were optimized in one dimension each, gave essentially identical results.

The S_2 to S_3 transition starts out by oxidizing P_{680}. Since a proton is left on OEC from the previous transition, this increases the redox potential of P_{680} by 0.22 V, see above. The increased driving force is used to release a proton from the OEC by charge repulsion. The proton released, like in all the other S-transitions, is one on the water ligand (position **C**) on **Mn4**. As seen in Fig. 10, the proton release is now exergonic by 3.4 kcal/mol. The release is experimentally found to be associated with a substantial barrier. The release time is 200 μ-sec corresponding to a barrier of 10–12 kcal/mol. This time might be long enough to affect the back-reaction of the initial charge separation in the reaction center. The endergonicity of the back-reaction could be reduced from 14 kcal/mol [71] down to only 9 kcal/mol, but the situation should be analyzed in more detail. To computationally determine the barrier for proton release would require much larger models and has therefore not been attempted.

The proton release is followed by an electron release, endergonic by 6.7 kcal/mol, leading to an oxidation of **Mn1**. This oxidation leads to firm binding of the water molecule with a change of the **Mn1**–O distance from 2.40 Å to 1.81 Å, due to the loss of the Jahn–Teller axis on this center. It is proposed that the large reconstruction implicated by

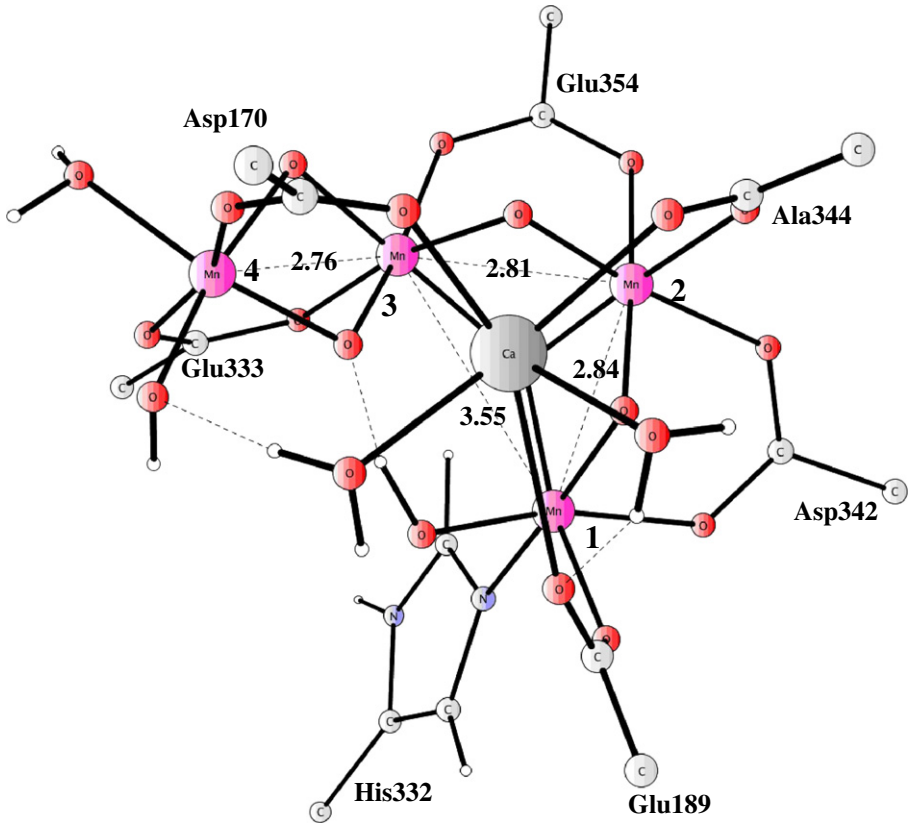

Fig. 11. Optimized S_3^0 structure. Only most essential atoms are shown.

several experiments in the S_2 to S_3 concerns this change. The oxidation of **Mn1** is directly followed by a proton transfer from the bound water from **A** to **B**, which is strongly exergonic by 10.7 kcal/mol. The large exergonicity is expected since **Mn1** has been oxidized. As in the previous study, the reverse order of these steps was tried, but also here found to require a higher barrier. There remains a possibility that the electron release to Tyr_Z is concerted with the proton transfer. To test this a larger model including Tyr_Z would obviously be required. Still, since the rate of this step is anyway quite fast, a concerted mechanism would not change any conclusions. The next step is a proton transfer from **B** to **C**, with a low barrier of 5.9 kcal/mol, and exergonic by 4.0 kcal/mol. The ground state for S_3 is now reached with the optimized structure shown in Fig. 11. As in the S_2 to S_3 transition, it is endergonic to remove the next proton from the OEC. This time the endergonicity of 2.1 kcal/mol is parameterized to match experimental observations for the S_3 to S_4 transition [55,56], see above. Note that this is the only experimental parameter used in the energy diagrams except the total driving force.

The Mn–Mn distances in S_3 are **Mn1**–**Mn2** = 2.84 Å (2.83 Å), **Mn1**–**Mn3** = 3.55 Å (3.46 Å), **Mn2**–**Mn3** = 2.81 Å (2.80 Å), and **Mn3**–**Mn4** = 2.76 Å (2.74 Å), with the S_2 distances in parenthesis. These results are very similar to the ones obtained in the previous study. As expected, the protonation state of His337 has almost no effect on these distances.

The computed Mn–Mn distance-changes in the S_2 to S_3 transition can be compared to EXAFS measurements. In the EXAFS studies by Yachandra et al. [62–64], three short distances with 2.73 Å, 2.73 Å and 2.82 Å were found in S_2 in reasonable agreement with the calculated distances 2.74 Å, 2.80 Å, and 2.83 Å, taking into account that B3LYP-distances are generally somewhat long. The fourth distance was 3.30 Å. In the EXAFS study by Dau et al. [6], only two short Mn–Mn distances with 2.69 Å and 2.74 Å were suggested. The other two were claimed to be longer than 3 Å. The present result for the long distance is 3.46 Å. For the changes of the short Mn–Mn distances in the S_2 to S_3 transition, there are different conclusions in the two EXAFS studies. In the studies by Yachandra et al., it was concluded that there is a lengthening of one of the 2.73 Å distances to 2.80 Å, and also of the 2.82 Å distance to 3.00 Å. In the study by Dau et al. it was suggested that there is a formation of an additional 2.7 Å Mn–Mn bis-μ-oxo bridge in S_3, leading to three short distances with 2.73 Å, 2.77 Å and 2.80 Å. Perhaps the most noteworthy of the differences of the S_3 distances is the one which is 2.80 Å in the Dau et al. study, and as long as 3.0 Å in the Yachandra et al. study. The two different proposals led to quite different proposals for the water oxidation mechanism. Surprisingly, the present calculations show almost no change of the Mn–Mn distances, and therefore do not support any of the experimental suggestions. It can be noted that the present result is in good agreement with the studies of Yachandra et al. for the S_2 state, while it is in good agreement with the one of Dau et al. for the S_3 state. However, there is agreement on the point that there is a significant structural change in this transition, which in the present case only concerns a large change of one of the Mn–O distances due to the disappearance of a Jahn–Teller axis. An analysis of the EXAFS spectrum has recently been initiated but is not quite finished yet. At the present stage it appears that the main part of the discrepancies between theory and experiments are due to which atoms are allowed to contribute to the spectra. In the theoretical calculations of the spectra, the full model has been allowed to contribute, while in the experimental analysis the contributions from the ligands and the surrounding was more approximate, mainly because at the time of the experiments, the positions of the ligands and the overall structure of the surrounding of the OEC were not known. Still, minor actual discrepancies between theory and experiments cannot be excluded.

Different experimental types of interpretations of NEXAFS (XANES) spectra have led to significantly different pictures of the S_2 to S_3 transition, and therefore dramatically influenced the suggested mechanisms for O—O bond formation. In one type of interpretation the shift of the absorption edge was concluded to indicate a ligand centered oxidation rather than a manganese centered one [72]. In another type of interpretation, using a very similar measured spectrum, the oxidation was instead concluded to be manganese centered [73]. Which type of interpretation should be used is not clear from model studies. In the former study the position of the edge was determined by the zero crossing of the second derivative of the absorption threshold. In the latter it was determined as the energy at half intensity of the rising curve. A computational study simulating the spectra from the present type of structures was recently done [25]. As described above, the present S_2 to S_3 transition is purely manganese centered. The experimental spectrum was well reproduced using a ΔSCF DFT procedure, showing that this transition should be described as an Mn(III) to Mn(IV) oxidation. However, if the same procedures as used experimentally to determine the edge shifts were adopted, the interpretations become as different as in the experimental papers. Apparently, to determine the position of the edge by the zero crossing of the second derivative of the absorption threshold does not work in the present case. Overall, NEXAFS does not appear to be a reliable method to determine oxidation states, at least without a careful computational analysis. Connected with this problem of analysis, is the fact that oxidation of a metal in a metal complex hardly changes the charge on the metal [74].

3.4. The S_3 to S_4 transition

Also the S_3 to S_4 transition has been described in detail in the previous study [19]. The transition starts out by oxidizing P_{680} and the positive charge leads to a release of a proton from the OEC by repulsion. The exergonicity is 2.9 kcal/mol, see Fig. 12. At this stage the OEC should be oxidized. Since all manganese now are in an Mn(IV)-state, the oxidation

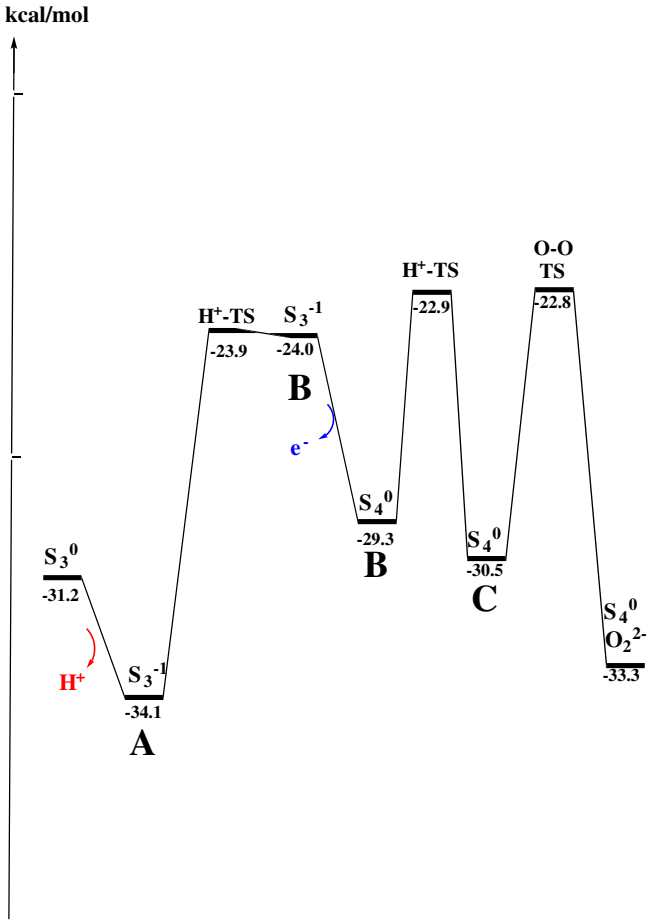

Fig. 12. Energy diagram for the S_3 to S_4 transition. The labels **A–C** indicate the positions of the moving proton, see Fig. 2.

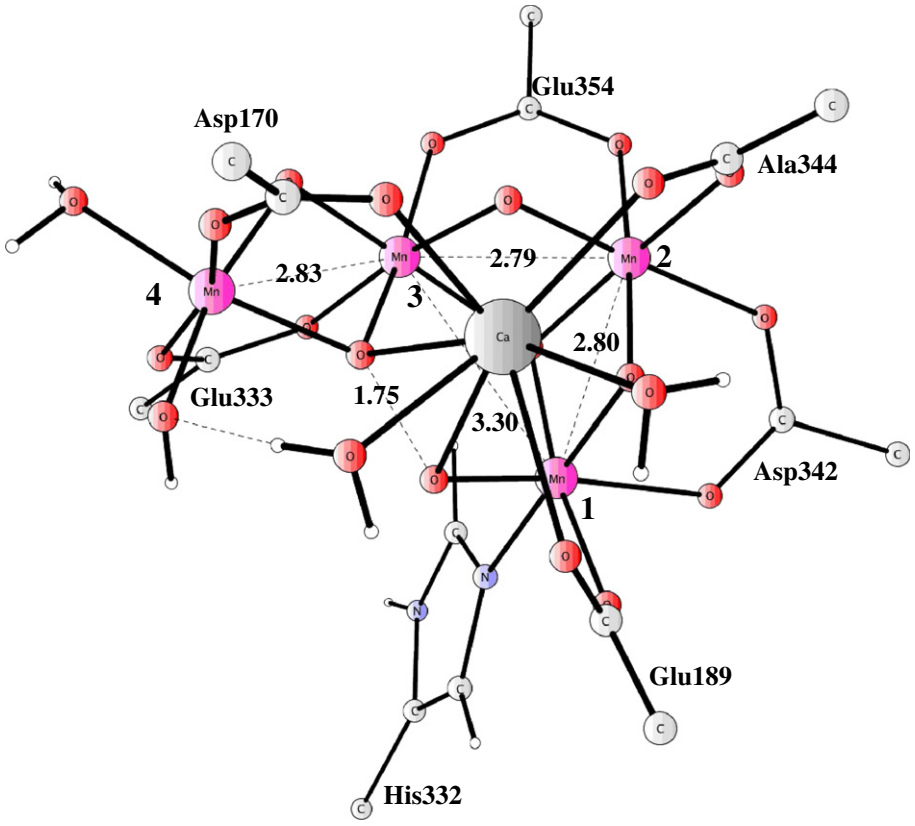

Fig. 13. Optimized transition state for O—O bond formation. Only most essential atoms are shown.

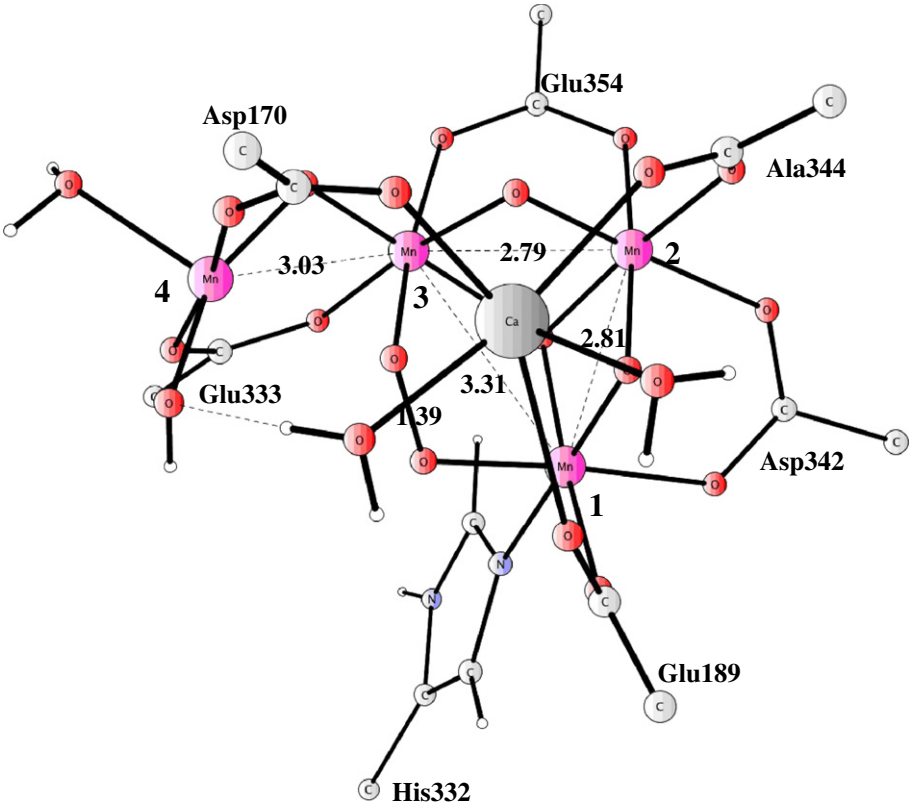

Fig. 14. Optimized peroxide product. Only most essential atoms are shown.

has to occur for a ligand. To make the oxidation possible the proton on the hydroxyl group on **Mn1** has to be removed, by a transfer from position **A** to **B**. This step is endergonic by 10.1 kcal/mol and goes over barrier with almost the same energy. This means that the step from S_3^{-1}(**A**) to S_4^0(**B**), see figure, can be regarded as one concerted PCET (proton coupled electron transfer) step. At this point the oxo group at position **A** can be oxidized to an oxyl radical, which is absolutely necessary for forming the O—O bond. This oxidation is exergonic by 5.3 kcal/mol. Still another proton transfer, from **B** to **C**, has to occur to create optimal conditions for O—O bond formation. The reason for this transition is that in the O—O bond forming step, **Mn4** will be reduced to Mn(III), which requires a JT-axis pointing at the substrate oxygen on this metal. Water is an ideal ligand along this axis. This proton transfer is slightly exergonic by 1.2 kcal/mol and goes over a barrier of 6.4 kcal/mol. A spin of 0.73 is now present on the two oxygens forming the O—O bond, with 0.62 on one and 0.11 on the other oxygen. The transition states for both proton transfers were discussed in detail in the previous paper [19].

The mechanism for O—O bond formation was also discussed in detail in the previous papers [18,19] and is very similar to the one suggested already 2006 [12]. The spins are alternating with antiferromagnetic coupling between **Mn1** and **Mn4**, and opposite spins on the two oxygens forming the bond. The local barrier is 7.7 kcal/mol and the transition state is shown in Fig. 13. Since S_3^{-1} with the proton on position **A** is the resting state which lies 3.6 kcal/mol lower than the immediate reactant for O—O bond formation, the actual barrier is 11.3 kcal/mol. It should be noted that the barrier for proton transfer from **B** to **C** is almost as high. O—O bond formation is exergonic by 2.8 kcal/mol from **C**. The peroxide is shown in Fig. 14. At this stage, **Mn4** is Mn(III), the other ones still Mn(IV).

In another mechanism suggested for O—O bond formation in the OEC, Arg357 plays a key role for proton transfer or as a base [30]. To test the hypothesis of an intermediate unprotonated Arg357, two different protonation states of the S_3^{-1} state was studied, which is the most relevant state to look at. In the first of them, there is an hydroxide at position **C** of **Mn4** and a protonated Arg357, which is the ground state obtained here for that state (the one with energy −34.1 kcal/mol in Fig. 12). The hydroxide was created by removing a proton from water in position **C** on **Mn4** in the ground state of S_3^0 (with energy −31.2 kcal/mol in the diagram). In the second one, a proton is instead removed from the protonated Arg357. The result is that the present ground state of S_3^{-1} is 12.0 kcal/mol (8.6 pK_a units) more stable. Removing a proton from the water on position **C** is thus very much more favorable than removing it from the protonated Arg357. This means that an unprotonated Arg357 is actually less likely than expected to be present as an intermediate in S_4, probably due to the stabilizing negative oxo groups on the OEC. If an unprotonated Arg357 were to be used in the O—O bond forming process, the calculated effect of 12 kcal/mol should be added to the computed barrier, at least using the present type of models. If also the cost of creating the oxyl radical is added, in the present mechanism 3.6 kcal/mol, a water attack mechanism of this type [30] would have a barrier higher than 20 kcal/mol, as found in all other studies using that mechanism [12].

3.5. The S_4 to S_0 transition

After the peroxide has been formed a quite complicated set of reaction steps starts for returning to the S_0-state. Some of these steps are actually also the hardest ones to describe using the present methodology, and the energetics is therefore probably less accurate than for the other transitions.

In the first step in this sequence, the peroxide is released with a large gain of entropy. Simultaneously, two manganese (**Mn1** and **Mn3**) are reduced from Mn(IV) to Mn(III). The previous model with an unprotonated His337, gave an unreasonable endergonicity for this step of +12 kcal/mol. If this was a true value, this step would be clearly rate-limiting and much too slow compared to experiments. There are two possibilities to correct this deficiency in the description. The first one is to try to see if the substrate water molecule that should enter before the ground state of S_0 is reached, enters concertedly with O_2 release. A large effort was spent trying to find this type of concerted pathway, but without success. There was never any sign of a gain in energy by letting the water enter early. The second possibility to correct the result is to change the model. Since all other steps are extremely well reproduced by the present model, the change in the model should be as small as possible. By letting His337 be protonated, the reduction of the two manganese obviously becomes easier in absolute values. However, only relative redox potentials count in the energy diagram, and to reach an effect the other steps should be less affected by the protonation. It turns out that this is the case, and only the O_2 release step changes significantly if relative redox potentials are used, as seen by comparing the present diagrams to the ones obtained using the unprotonated His337 [19] The endergonicity of O_2 release is now reduced to a more reasonable value of +4.5 kcal/mol, see Fig. 15. Even if this modification corrects the problem for O_2 release, a more complicated solution to the problem involving protein structural changes should still be left open.

After O_2 is released, a water on calcium moves towards the cavity in the center of the OEC as shown in Fig. 16. To reach the ground state for S_0, a proton first has to be transferred from the calcium bound water to the hydroxide group at position **B** on **Mn4**. The transition

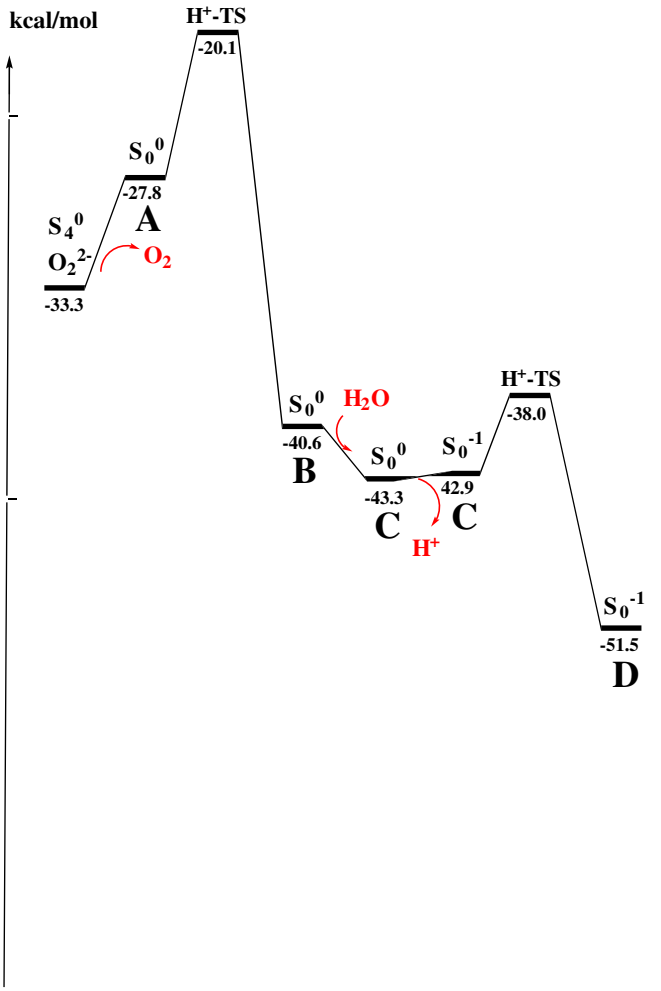

Fig. 15. Energy diagram for the S_4 to S_0 transition. The labels A–C indicate the positions of the moving proton, see Fig. 2.

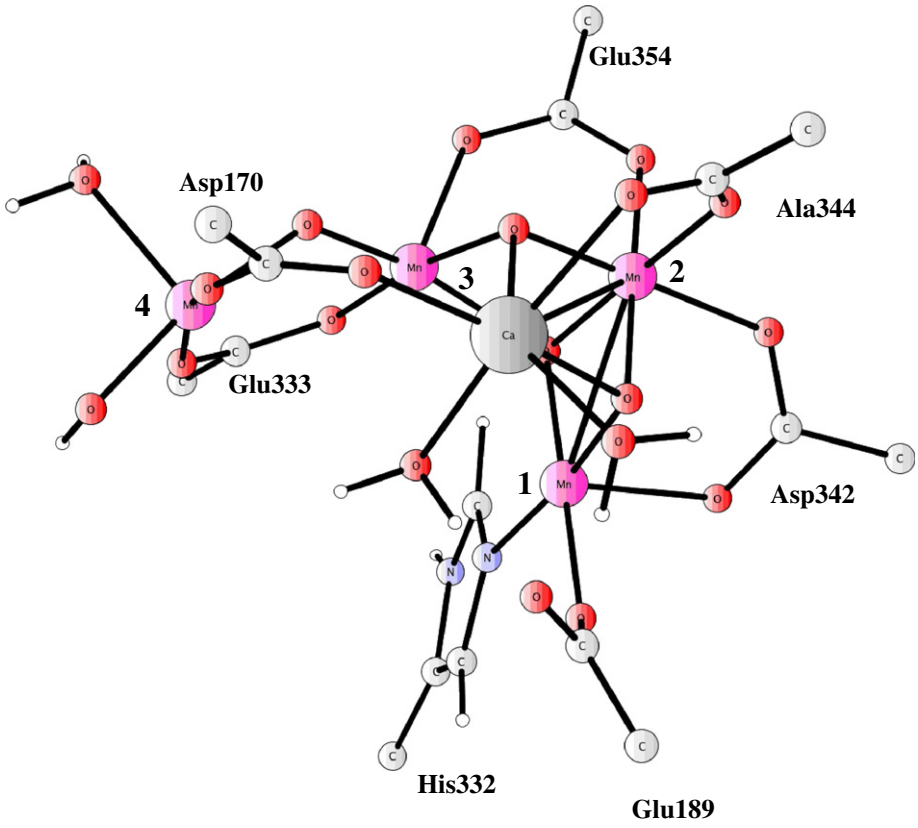

Fig. 16. S_0^0 structure obtained after O_2 is released and the new water substrate binds. Only most essential atoms are shown.

state is shown in Fig. 17. The barrier for this step is 7.7 kcal/mol, reaching an energy of −20.1 kcal/mol at the TS, see Fig. 15. This is the highest point in the S_3 to S_0 transition and should in principle be rate limiting for water oxidation. However, the uncertainty of this value makes this conclusion questionable. Since the key chemistry is the formation of the O—O bond, that step is much more likely to be rate limiting. The calculated energy values at the respective TS are anyway quite close, −20.1 kcal/mol and −22.8 kcal/mol. The proton transfer step is exergonic by as much as 12.8 kcal/mol. At this stage a proton is released from the water at position **C** on **Mn4**. This is followed by the binding of a substrate water with an estimated binding energy of 2.7 kcal/mol. Only one step remains to return to the start of the water oxidation cycle, see Fig. 4, and this is a proton transfer from the water on position **B** to the hydroxide on position **C**. The transition state is shown in Fig. 18 and it has a barrier of 4.9 kcal/mol and an exergonicity of 8.6 kcal/mol.

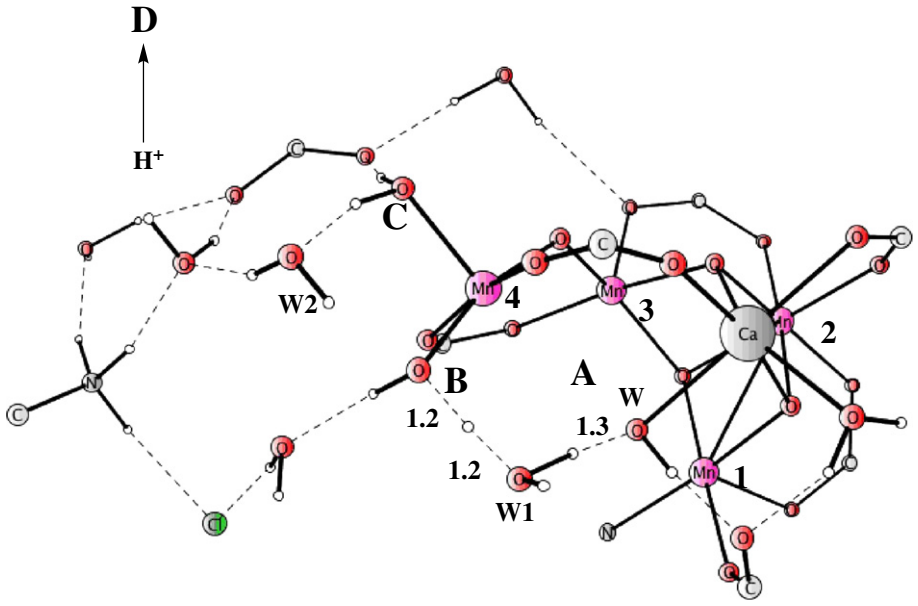

Fig. 17. Proton transfer transition state in S_0^0. Only most essential atoms are shown.

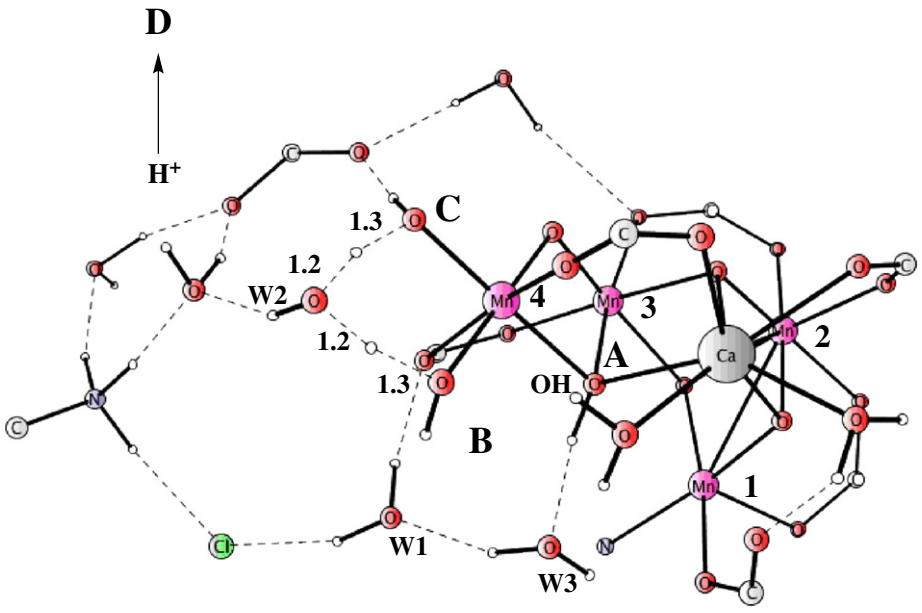

Fig. 18. Proton transfer transition state in the S_0^{-1}-state. Only most essential atoms are shown.

3.6. The full cycle, S_0 back to S_0

The energetic results discussed above are collected in the full diagram shown in black in Fig. 19. In this diagram, the individual proton transfer steps are removed. When this is done, O—O bond formation is rate limiting with a barrier from the resting S_3^{-1}-state of 11.3 kcal/mol (34.1 - 22.8). An important point about the mechanism is, of course, that protons and electrons are removed in an alternating fashion. This has been done also in the earlier DFT studies, see for example Ref. [10]. This preserves the charge of the catalyst as much as possible, which has been found to be an energetic advantage in enzyme mechanisms in general [15]. More recently, the model with alternating removal of charges has been used experimentally to analyze water oxidation in PSII, and has been found to explain a large body of experimental results [75]. The mechanism in the figure is in agreement with experiments as to when the protons and electrons are released from the OEC, and when the two substrate water molecules enter, one in S_0 and one in S_2. It agrees also with the fact that only an electron is released in the S_1 to S_2 transition. The total driving force is taken from experiments, and one parameter is fitted to observations of the proton release in the early part of the S_3 to S_4 transition.

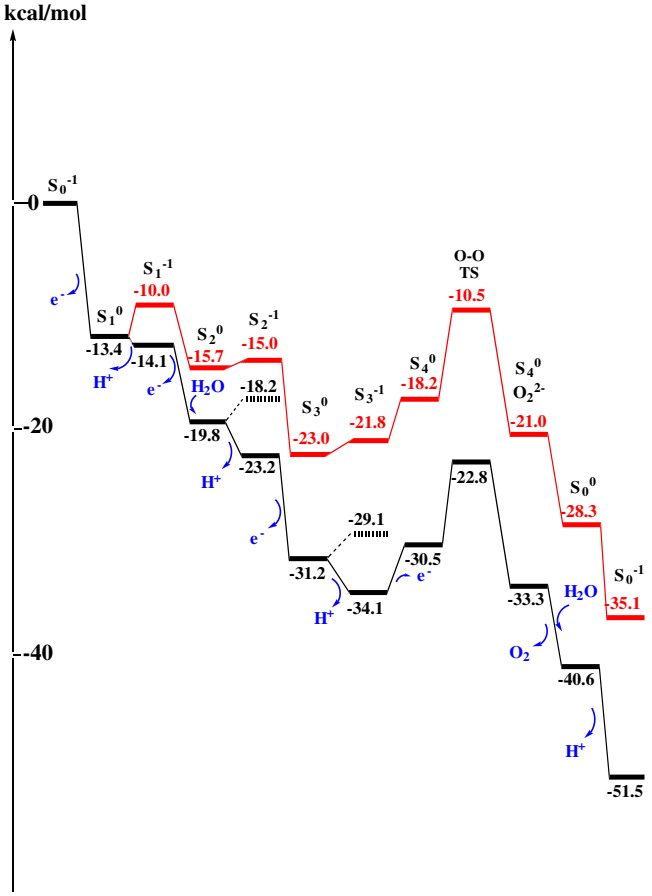

Fig. 19. Full energy diagram for water oxidation from S_0 back to S_0. The upper curve is with a full membrane gradient.

Also shown in the figure in red are the results when a full pH-gradient of 3 pH-units is applied. This means that 4.1 kcal/mol is added every time a proton is released. Remarkably, the membrane gradient only increases the barrier for the rate-limiting step to 12.5 kcal/mol from 11.3 kcal/mol, even though the driving force is reduced from 51.5 kcal/mol to 35.1 kcal/mol.

4. Conclusions

Energy diagrams and structures have for the first time been obtained for the full sequence of proton and electron release steps in water oxidation in photosystem II. The manganese centers are oxidized in the order **Mn3**, **Mn4** and **Mn1**. **Mn2** is always Mn(IV). In the S_3 to S_4 transition a terminal oxygen on Mn1 is oxidized. For the proton release steps, also transition states have been optimized for the microsteps. The energetics fits very well to observations. To obtain a reasonable energy for the O_2 release step, it was found necessary to protonate His337. Another change compared to previous studies is that a larger driving force is used for the last two S-transitions than for the first two. The argument for this follows from two experimental observations. One is that only an electron leaves the OEC in the S_1 to S_2 transition [60,61], and the second one is that a proton is released early in the S_3 to S_4 transition when P_{680} is oxidized [55,56].

The mechanism for O—O bond formation is essentially the same as the one suggested 2006 [12]. An oxyl radical in the center of the

OEC forms the O—O bond with a bridging oxo-group. In 2008, a structure of the resting state of the OEC was obtained starting from that transition state for O—O bond formation and adding electrons and protons [13]. That structure turned out to be very similar to the 2011 high-resolution X-ray structure [16]. The only notable difference was associated with a misplacement of Asp170. DFT studies performed after the 2011 structure, confirmed the expectation that the different position of Asp170 did only have very small effects on the mechanism for O—O bond formation [18].

Very recently important spectroscopic measurements have confirmed key elements of the present mechanism. First, using a combination of EPR, ENDOR, and DFT a structure of the S_2-state was reached [20] in almost exact agreement with one obtained independently by energy minimization based on the old DFT structure modified by the position of Asp170 [18]. Second, using W-band ^{17}O-ELDOR detected NMR spectroscopy, information about the two substrate positions were obtained, strongly suggesting the positions given by the present mechanism [21]. A very interesting future possibility would be if the experimental time resolution could be improved slightly to confirm the surprising changes in the water exchange rates in S_1 and S_2.

Supplementary data to this article can be found online at http://dx.doi.org/10.1016/j.bbabio.2012.10.006.

References

[1] K.N. Ferreira, T.M. Iverson, K. Maghlaoui, J. Barber, S. Iwata, Architecture of the photosynthetic oxygen evolving center, Science 303 (2004) 1831–1838.
[2] B. Loll, J. Kern, W. Saenger, A. Zouni, J. Biesiadka, Towards complete cofactor arrangement in the 3.0 Å resolution structure of photosystem II, Nature 438 (2005) 1040–1044.
[3] A. Guskov, J. Kern, A. Gabdulkhakov, M. Broser, A. Zouni, W.J. Saenger, Location of chloride and its possible functions in oxygen-evolving photosystem II revealed by X-ray crystallography, Nat. Struct. Biol. 16 (2009) 334–341.
[4] J. Yano, J. Kern, K.-D. Irrgang, M.J. Latimer, U. Bergmann, P. Glatzel, Y. Pushkar, J. Biesiadka, B. Loll, K. Sauer, J. Messinger, A. Zouni, V.K. Yachandra, X-ray damage to the Mn–$_4$Ca complex in single crystals of photosystem II: a case study for metalloprotein crystallography, Proc. Natl. Acad. Sci. U. S. A. 102 (2005) 12047–12052.
[5] V.K. Yachandra, K. Sauer, M.P. Klein, Manganese cluster in photosynthesis: where plants oxidize water to dioxygen, Chem. Rev. 96 (1996) 2927–2950.
[6] M. Haumann, C. Muller, P. Liebisch, L. Iuzzolino, J. Dittmer, M. Grabolle, T. Neisius, W. Meyer-Klaucke, H. Dau, Structural and oxidation state changes of the photosystem II manganese complex in four transitions of the water oxidation cycle (S0 to S1, S1 to S2, S2 to S3, and S3, S4 to S0) characterized by X-ray absorption spectroscopy at 20 K and room temperature, Biochemistry 44 (2005) 1894–1908.
[7] P.E.M. Siegbahn, R.H. Crabtree, Manganese oxyl radical intermediates and O—O bond formation in photosynthetic oxygen evolution and a proposed role for the calcium cofactor in photosystem II, J. Am. Chem. Soc. 121 (1999) 117–127.
[8] P.E.M. Siegbahn, Theoretical models for the oxygen radical mechanism of water oxidation and of the water oxidizing complex of photosystem II, Inorg. Chem. 39 (2000) 2923–2935.
[9] M. Lundberg, P.E.M. Siegbahn, Theoretical investigations of structure and mechanism of the oxygen evolving complex in PSII, Phys. Chem. Chem. Phys. 6 (2004) 4772–4780.
[10] M. Lundberg, P.E.M. Siegbahn, The mechanism for dioxygen formation in PSII studied by quantum chemical methods, Photochem. Photobiol. Sci. 4 (2005) 1035–1043.
[11] P.E.M. Siegbahn, M. Lundberg, Hydroxide instead of bicarbonate in the structure of the oxygen evolving complex, J. Inorg. Biochem. 100 (2006) 1035–1040.
[12] P.E.M. Siegbahn, O—O bond formation in the S_4-state of the oxygen evolving center in photosystem II, Chem. Eur. J. 12 (2006) 9217–9227.
[13] P.E.M. Siegbahn, A structure consistent mechanism for dioxygen formation in photosystem II, Chem. Eur. J. 27 (2008) 8290–8302.
[14] P.E.M. Siegbahn, Structures and energetics for O_2 formation in photosystem II, Acc. Chem. Res. 42 (2009) 1871–1880.
[15] P.E.M. Siegbahn, M.R.A. Blomberg, Modeling of Mechanisms for Metalloenzymes Where Protons and Electrons Enter or Leave, in: K. Morokuma, J. Musaev (Eds.), Computational Modeling for Homogeneous Catalysis and Biocatalysis, Wiley-VCH, Germany, 2008, pp. 57–81.
[16] Y. Umena, K. Kawakami, J.-R. Shen, N. Kamiya, Crystal structure of oxygen-evolving photosystem II at a resolution of 1.9 Å, Nature 473 (2011) 55–60.
[17] J. Messinger, Evaluation of different mechanistic proposals for water oxidation in photosynthesis on the basis of Mn4OxCa structures for the catalytic site and spectroscopic data, Phys. Chem. Chem. Phys. 6 (2004) 4764–4771.
[18] P.E.M. Siegbahn, The effect of backbone constraints — the case of water oxidation by the oxygen evolving complex in photosystem II, Chemphyschem 12 (2011) 3274–3280.
[19] P.E.M. Siegbahn, Mechanisms for proton release during water oxidation in the S_2 to S_3 and S_3 to S_4 transitions in photosystem II, Phys. Chem. Chem. Phys. 14 (2012) 4849–4856.
[20] W. Ames, D.A. Pantazis, V. Krewald, N. Cox, J. Messinger, W. Lubitz, F. Neese, Theoretical evaluation of structural models of the S2 state in the oxygen evolving complex of photosystem II: protonation states and magnetic interactions, J. Am. Chem. Soc. 133 (2011) 19743–19757.
[21] L. Rapatskiy, N. Cox, A. Savitsky, W.M. Ames, J. Sander, M.M. Nowacyzk, M. Rögner, A. Boussac, F. Neese, J. Messinger, W. Lubitz, Detection of the water binding sites of the oxygen-evolving complex of photosystem II using W-band 17-O Eldor-detected NMR spectroscopy, J. Am. Chem. Soc. 134 (2012) 16619–16634.
[22] J. Barber, K.N. Ferreira, K. Maghlaoui, S. Iwata, Structural model of the oxygen-evolving centre of photosystem II with mechanistic implications, Phys. Chem. Chem. Phys. 6 (2004) 4737–4742.
[23] H. Ishikita, W. Saenger, B. Loll, J. Biesiadka, E.-W. Knapp, Energetics of a possible proton exit pathway for water oxidation in photosystem II, Biochemistry 45 (2006) 2063–2071.
[24] P. Gatt, R. Stranger, R.J. Pace, Application of computational chemistry to understanding the structure and mechanism of the Mn catalytic site in photosystem II — a review, J. Photochem. Photobiol. B Biol. 104 (2011) 80–93;
S. Petrie, P. Gatt, R. Stranger, R.J. Pace, Modelling the metal atom positions of the photosystem II water oxidising complex: a density functional theory appraisal of the 1.9 angstrom resolution crystal structure, Phys. Chem. Chem. Phys. 14 (2012) 11333–11343.
[25] B. Brena, H. Ågren, P.E.M. Siegbahn, Modeling near edge fine structure X-ray spectra of the manganese catalytic site for water oxidation in photosystem II, J. Am. Chem. Soc. (2012), http://dx.doi.org/10.1021/ja306794p.
[26] M. Kusunoki, Mono-manganese mechanism of the photosystem II water splitting reaction by a unique Mn4Ca cluster, Biochim. Biophys. Acta 1767 (2007) 484–492.
[27] M. Kusunoki, S1-state Mn4Ca complex of photosystem II exists in equilibrium between the two most-stable isomeric substates: XRD and EXAFS evidence, J. Photochem. Photobiol. B Biol. 104 (2011) 100–110.
[28] E.M. Sproviero, M.B. Newcomer, J.A. Gascon, E.R. Batista, G.W. Brudvig, V.S. Batista, The MoD-QM/MM methodology for structural refinement of photosystem II and other biological macromolecules, Photosynth. Res. 102 (2009) 455–470.
[29] E.M. Sproviero, J.A. Gascon, J.P. McEvoy, G.W. Brudvig, V.S. Batista, Quantum mechanics/molecular mechanics study of the catalytic cycle of water splitting in photosystem II, J. Am. Chem. Soc. 130 (2008) 3428–3442.
[30] E.M. Sproviero, J.A. Gascon, J.P. McEvoy, G.W. Brudvig, V.S. Batista, A model of the oxygen-evolving center of photosystem II predicted by structural refinement based on EXAFS simulations, J. Am. Chem. Soc. 130 (2008) 6728–6730.
[31] X. Li, E.M. Sproviero, U. Ryde, V.S. Batista, G. Chen, Theoretical EXAFS studies of a model of the oxygen-evolving complex of photosystem II obtained with the quantum cluster approach, Int. J. Quantum Chem. (2012), http://dx.doi.org/10.1002/qua.24143.
[32] J. Messinger, M. Badger, T. Wydrzynski, Detection of one slowly exchanging substrate water molecule in the S-3 state of photosystem II, Proc. Natl. Acad. Sci. 92 (1995) 3209–3213.
[33] V.L. Pecoraro, M.J. Baldwin, M.T. Caudle, W.-Y. Hsieh, N.A. Law, A proposal for water oxidation in photosystem II, Pure Appl. Chem. 70 (1998) 925–929.
[34] D.A. Pantazis, M. Orio, T. Petrenko, S. Zein, W. Lubitz, J. Messinger, F. Neese, Structure of the oxygen-evolving complex of photosystem II: information on the S_2 state through quantum chemical calculation of its magnetic properties, Phys. Chem. Chem. Phys. 11 (2009) 6788–6798.
[35] P.E.M. Siegbahn, An energetic comparison of different models for the oxygen evolving complex of photosystem II, J. Am. Chem. Soc. 131 (2009) 18238–18239.
[36] J. Yano, J. Kern, K. Sauer, M.J. Latimer, Y. Pushkar, J. Biesiadka, B. Loll, W. Saenger, J. Messinger, A. Zouni, V.K. Yachandra, Where water is oxidized to dioxygen: structure of the photosynthetic Mn4Ca cluster, Science 314 (2006) 821–825.
[37] H. Dau, A. Grundmeier, P. Loja, M. Haumann, On the structure of the manganese complex of photosystem II: extended-range EXAFS data and specific atomic-resolution models for four S-states, Philos. Trans. R. Soc. B 363 (2008) 1237–1244.
[38] N. Cox, L. Rapatskiy, J.-H. Su, D.A. Pantazis, M. Sugiura, L. Kulik, P. Dorlet, A.W. Rutherford, F. Neese, A. Boussac, W. Lubitz, J. Messinger, Effect of Ca2+/Sr2+ substitution on the electronic structure of the oxygen-evolving complex of photosystem II: a combined multifrequency EPR, Mn-55-ENDOR, and DFT study of the S2 State, J. Am. Chem. Soc. 133 (2011) 3635–3648.
[39] S. Schinzel, J. Schraut, A.V. Arbuznikov, P.E.M. Siegbahn, M. Kaupp, Density functional calculations of ^{55}Mn, ^{14}N and ^{13}C electron paramagnetic resonance parameters support an energetically feasible model for the S_2 state of the oxygen-evolving complex of photosystem II, Chem. Eur. J. 16 (2010) 10424–10438.
[40] S. Luber, I. Rivalta, Y. Umena, K. Kawakami, J.-R. Shen, N. Kamiya, D. Bruce, G.W. Brudvig, V.S. Batista, S1-state model of the O2-evolving complex of photosystem II, Biochemistry 50 (2011) 6308–6311.
[41] A. Grundmeier, H. Dau, Structural models of the manganese complex of photosystem II and mechanistic implications, Biochim. Biophys. Acta 1817 (2012) 88–105.
[42] A. Galstyan, A. Robertazzi, E.W. Knapp, Oxygen-evolving Mn cluster in photosystem II: the protonation pattern and oxidation state in the high-resolution crystal structure, J. Am. Chem. Soc. 134 (2012) 7442–7449.
[43] I. Rivalta, M. Amin, S. Luber, S. Vassiliev, R. Pokhrel, Y. Umena, K. Kawakami, J.-R. Shen, N. Kamiya, D. Bruce, G.W. Brudvig, M.R. Gunner, V.S. Batista, Structural–functional role of chloride in photosystem II, Biochemistry 50 (2011) 6312–6315.
[44] A.D. Becke, Density-functional thermochemistry. III. The role of exact exchange, J. Chem. Phys. 98 (1993) 5648–5652.
[45] M. Reiher, O. Salomon, B.A. Hess, Reparameterization of hybrid functionals based on energy differences of states of different multiplicity, Theor. Chem. Acc. 107 (2001) 48–55.
[46] P.E.M. Siegbahn, The performance of hybrid DFT on mechanisms involving transition metal complexes in enzymes, J. Biol. Inorg. Chem. 11 (2006) 695–701.

[47] P.E.M. Siegbahn, F. Himo, Recent developments of the quantum chemical cluster approach for modeling enzyme reactions, J. Biol. Inorg. Chem. 14 (2009) 643–651.
[48] P.E.M. Siegbahn, F. Himo, The quantum chemical cluster approach for modeling enzyme reactions, in: Wiley Interdisciplinary Reviews: Computational Molecular Science, vol. 1, 2011, pp. 323–336.
[49] S. Grimme, Semiempirical hybrid density functional with perturbative second-order correlation, J. Chem. Phys. 124 (2006) 034108;
T. Schwabe, S. Grimme, Double-hybrid density functionals with long-range dispersion corrections: higher accuracy and extended applicability, Phys. Chem. Chem. Phys. 9 (2007) 3397–3406.
[50] Jaguar 7.0, Schrödinger, LLC, New York, NY, 2007.
[51] P.E.M. Siegbahn, Recent theoretical studies of water oxidation in photosystem II, J. Photochem. Photobiol. B Biol. 104 (2011) 94–99.
[52] L. Noodleman, D.A. Case, Density-functional theory of spin polarization and spin coupling in iron–sulfur clusters, Adv. Inorg. Chem. 38 (1992) 423–470.
[53] B.A. Diner, Amino acid residues involved in the coordination and assembly of the manganese cluster of photosystem II. Proton-coupled electron transport of the redox-active tyrosines and its relationship to water oxidation, Biochim. Biophys. Acta 1503 (2001) 147–163.
[54] F. Rappaport, J. Lavergne, Coupling of electron and proton transfer in the photosynthetic water oxidase, Biochim. Biophys. Acta 1503 (2001) 246–259.
[55] F. Rappaport, M. Blanchard-Desce, J. Lavergne, Kinetics of electron transfer and electrochromic change during the redox transitions of the photosynthetic oxygen-evolving complex, Biochim. Biophys. Acta 1184 (1994) 178–192.
[56] M. Haumann, P. Liebisch, C. Müller, M. Barra, M. Grabolle, H. Dau, Photosynthetic O2 formation tracked by time-resolved X-ray experiments, Science 310 (2005) 1019–1021.
[57] J. Messinger, G. Renger, Photosynthetic Water Splitting, in: G. Renger (Ed.), Primary Processes of Photosynthesis: Principles and Apparatus, Comprehensive Series in Photochemical and Photobiological Sciences, vol. 9 (Part 2), RSC Publishing, Cambridge, UK, 2008, pp. 291–349.
[58] G. Han, F. Mamedov, S. Styring, Misses during water oxidation in photosystem II are S state-dependent, J. Biol. Chem. 287 (2012) 13422–13429.
[59] P.E.M. Siegbahn, M.R.A. Blomberg, On the proton pumping mechanism in cytochrome c oxidase, J. Phys. Chem. A 112 (2008) 12772–12780.
[60] G. Renger, Mechanistic and structural aspects of photosynthetic water oxidation, Physiol. Plant. 100 (1997) 828–841.
[61] V. Förster, W. Junge, Stoichiometry and kinetics of proton release upon photosynthetic water oxidation, Photochem. Photobiol. 41 (1985) 183–190.
[62] W. Liang, T.A. Roelofs, R.M. Cinco, A. Rompel, M.J. Latimer, W.O. Yu, K. Sauer, M.P. Klein, V.K. Yachandra, Structural change of the Mn cluster during the S_2 to S_3 state transition of the oxygen-evolving complex of photosystem II. Does it reflect the onset of water/substrate oxidation? Determination by Mn X-ray absorption spectroscopy, J. Am. Chem. Soc. 122 (2000) 3399–3412.
[63] J.H. Robblee, J. Messinger, R.M. Cinco, K.L. McFarlane, C. Fernandez, S.A. Pizarro, K. Sauer, V.K. Yachandra, The Mn cluster in the S-0 state of the oxygen-evolving complex of photosystem II studied by EXAFS spectroscopy: are there three di-mu-oxo-bridged Mn-2 moieties in the tetranuclear Mn complex? J. Am. Chem. Soc. 124 (2002) 7459–7471.
[64] Y. Pushkar, J. Yano, P. Glatzel, J. Messinger, A. Lewis, K. Sauer, U. Bergmann, V.K. Yachandra, J. Biol. Sci. 282 (2006) 7198–7208.
[65] W. Hillier, T. Wydrzynski, Substrate water interactions within the Photosystem II oxygen evolving complex, Phys. Chem. Chem. Phys. 6 (2004) 4882–4889.
[66] G.C. Dismukes, Y. Siderer, Intermediates of a polynuclear manganese center involved in photosynthetic oxidation of water, Proc. Natl. Acad. Sci. 7851 (1981) 274–278.
[67] A. Boussac, J.-J. Girerd, A.W. Rutherford, Conversion of the spin state of the manganese complex in photosystem II induced by near-infrared light, Biochemistry 35 (1996) 6984–6989.
[68] D.A. Pantazis, W. Ames, N. Cox, W. Lubitz, F. Neese, Two interconvertible structures explain the spectroscopy of the oxygen evolving complex in its S2 state, Angew. Chem. Int. Ed. 51 (2012) 9935–9940.
[69] H. Suzuki, M. Sugiura, T. Noguchi, Monitoring water reactions during the S-state cycle of the photosynthetic water-oxidizing center: detection of the DOD bending vibrations by means of Fourier transform infrared spectroscopy, Biochemistry 47 (2008) 11024–11030.
[70] I.L. McConnell, V.M. Grigoryants, C.P. Scholes, W.K. Myers, P.-Y. Chen, J.W. Whittaker, G.W. Brudvig, EPR-ENDOR characterization of (O-17, H-1, H-2) water in manganese catalase and its relevance to the oxygen-evolving complex of photosystem II, J. Am. Chem. Soc. 134 (2012) 1504–1512.
[71] M.R.A. Blomberg, P.E.M. Siegbahn, G.T. Babcock, Modeling electron transfer in biochemistry: a quantum chemical study of charge separation in *Rhodobacter Sphaeroides* and Photosystem II, J. Am. Chem. Soc. 120 (1998) 8812–8824.
[72] J. Messinger, J.H. Robblee, U. Bergmann, C. Fernandez, P. Glatzel, H. Visser, R.M. Cinco, K.L. McFarlane, E. Bellacchio, S.A. Pizarro, S.P. Cramer, K. Sauer, M.P. Klein, V.K. Yachandra, Absence of Mn-centered oxidation in the S2 to S3 transition: implications for the mechanism of photosynthetic water oxidation, J. Am. Chem. Soc. 123 (2001) 7804–7820.
[73] L. Iuzzolino, J. Dittmer, W. Dörner, W. Meyer-Klaucke, H. Dau, X-ray absorption spectroscopy on layered photosystem II membrane particles suggests manganese-centered oxidation of the oxygen-evolving complex for the S0–S1, S1–S2, and S2–S3 transitions of the water oxidation cycle, Biochemistry 37 (1998) 17112–17119.
[74] P.E.M. Siegbahn, R.H. Crabtree, The mechanism of C–H activation by Di-iron methane monooxygenases: quantum chemical studies, J. Am. Chem. Soc. 119 (1997) 3103–3113.
[75] H. Dau, M. Haumann, Eight steps preceding O—O bond formation in oxygenic photosynthesis — a basic reaction cycle of the photosystem II manganese complex, Biochim. Biophys. Acta 1767 (2007) 472–483.